Sadaki *et al. Skeletal Muscle* (2025) 15:19
https://doi.org/10.1186/s13395-025-00391-5

Skeletal Muscle

RESEARCH Open Access

Large MAF transcription factors reawaken evolutionarily dormant fast-glycolytic type IIb myofibers in human skeletal muscle

Shunya Sadaki[1], Ryosuke Tsuji[1], Takuto Hayashi[1,2], Masato Watanabe[1], Ryoto Iwai[1], Gu Wenchao[3], Ekaterina A. Semenova[4,5], Rinat I. Sultanov[4], Andrey V. Zhelankin[4], Edward V. Generozov[4], Ildus I. Ahmetov[4,6,7], Iori Sakakibara[8], Koichi Ojima[9], Hidetoshi Sakurai[10], Masafumi Muratani[11], Takashi Kudo[1], Satoru Takahashi[1] and Ryo Fujita[12*]

Abstract

Background Small mammals such as mice rely on type IIb myofibers, which express the fast-contracting myosin heavy chain isoform *Myh4*, to achieve rapid movements. In contrast, larger mammals, including humans, have lost MYH4 expression. Thus, they favor slower-contracting myofiber types. However, the mechanisms underlying this evolutionary shift remain unclear. We recently identified the large Maf transcription factor family (*Mafa*, *Mafb*, and *Maf*) as key regulators of type IIb myofiber specification in mice. In this study, we investigate whether large MAFs play a conserved role in the induction of MYH4 expression and glycolytic metabolism in human and bovine skeletal muscle.

Methods We performed adenovirus-mediated overexpression of large MAFs in iPSC-derived human myotubes and primary bovine myotubes. We subsequently quantified MYH4 expression using RT-qPCR, RNA sequencing (RNA-seq), and LC-MS/MS analysis. Glycolytic capacity was assessed using a flux analyzer and metabolic gene expression profiling. Additionally, RNA-seq analysis of human muscle biopsy samples was conducted to determine the correlations between large MAFs and the expression of MYH4 and other myosin genes, as well as their association with fast fiber composition and athletic training.

Results Overexpression of large MAFs in human and bovine myotubes robustly induced *MYH4* expression, with mRNA levels increasing by 100- to 1000-fold. LC-MS/MS analysis provided clear evidence of MYH4 protein expression in human myotubes, where it was previously undetectable. RNA-seq and flux analyzer data revealed that large MAFs significantly enhanced glycolytic capacity by upregulating the expression of key genes involved in glucose metabolism. Moreover, RNA-seq analysis of human muscle biopsy samples revealed a positive correlation between *MAFA*, *MAF*, and *MYH4* expression. Furthermore, *MAFA* and *MAF* expression levels were elevated in power-trained individuals, accompanied by increased expression of *MYH4* and other fast myosin genes.

*Correspondence:
Ryo Fujita
fujiryo@md.tsukuba.ac.jp

Full list of author information is available at the end of the article

Conclusions Our findings establish large MAF transcription factors as key regulators of *MYH4* expression and glycolytic metabolism in human skeletal muscle. This discovery provides novel insights into the evolutionary loss of type IIb myofibers in larger mammals and suggests potential strategies for enhancing muscle performance and

Background

Skeletal muscles are composed of myofibers with distinct contractile, metabolic, and fatigue-resistant properties, as well as differing vulnerabilities in pathophysiological conditions [1, 2]. Myofibers are classified as slow-twitch (type I) and fast-twitch (type II). Type I myofibers are rich in mitochondria, exhibit high oxidative metabolism, and express slow isoforms of sarcomeric proteins, such as myosin heavy chain 7 (*Myh7*). Type II myofibers are further divided into type IIa, IIx, and IIb based on the expression of the Myh isoforms *Myh2*, *Myh1*, and *Myh4*, respectively. Each myosin isoform exhibits different ATPase activities that correlate with muscle contraction speed. Fast myofibers that express *Myh4* contract at greater speeds than those expressing *Myh1*, *Myh2*, and *Myh7*, consequently generating up to ten times more power than slow myofibers [3, 4]. Additionally, type IIb myofibers have an underdeveloped mitochondrial network and high concentrations of glycolytic enzymes, thereby supporting active glycolysis for ATP production.

Skeletal muscle is the most abundant tissue in adult humans, accounting for approximately 40% of the total body mass. Consequently, the proportion of myofiber types affects muscle performance and whole-body metabolism. In addition, it affects susceptibility to conditions such as diabetes [5, 6] and the progression of muscular dystrophy [7, 8]. Myofiber composition can be remodeled in response to various pathophysiological conditions, including exercise, disuse, diabetes, space travel, and aging. During disuse-induced muscle atrophy, as observed in space travel, a slow-to-fast type IIb conversion is exhibited in the mouse soleus muscle, which primarily consists of type I and type IIa myofibers [9, 10]. Conversely, aerobic exercise can activate slow muscle gene programs, including PGC-1α, in rodents [11–13]. Myofiber types substantially change with aging. Aging induces a type IIb-to-IIx shift in fast muscles and a type IIa-to-I shift in slow muscles in rodent skeletal muscle. This results in an overall fast-to-slow myofiber type transition [14, 15]. Human type II myofibers are more prone to myonuclear apoptosis and atrophy with aging, leading to a fast-to-slow transition in sarcopenic muscle [16, 17]. This may contribute to decreased locomotor activity in the elderly. However, the mechanistic role of myofiber type shifts in human skeletal muscle pathogenesis, including aging, remains largely unknown.

The expression of Myh isoforms is highly diverse across animal species. In particular, a notable difference in *Myh4* expression has been observed between large and small mammals [16, 18–20]. Small animals such as rodents contain the full spectrum of myofiber types, namely, type I, IIa, IIx, and IIb myofibers. In contrast, the skeletal muscles of larger animals, including humans, typically lack type IIb myofibers and exhibit low or undetectable *MYH4* expression at the transcriptional level [20, 21]. Human skeletal muscles primarily consist of type I, IIa, and IIx fibers expressing the corresponding *MYH7*, *MYH2*, and *MYH1* genes. Recent proteomic studies suggest that in many individuals, pure type IIx fibers are rare and predominantly exist as IIx/IIa hybrid myofibers [22, 23]. A small subset of specialized muscles, such as extraocular muscles, exhibit detectable levels of *MYH4* mRNA; however, the MYH4 protein remains undetectable [24, 25]. As large animals retain *MYH4*, we hypothesized that they could develop type IIb myofibers by activating *MYH4* expression. Type IIb myofibers enable rapid contraction, are larger than other myofibers, and generate a strong force with high glycolytic activity [17, 26]. Therefore, understanding how large animals lost *MYH4* expression during evolution could provide insights into muscle function and adaptation across species, particularly as it relates to physiological and metabolic demands unique to large animals.

The adult fast myosin (fMyh) genes *Myh2*, *Myh1*, *Myh4* are clustered on chromosomes 11 and 17 in mice and humans, respectively. Dos Santos et al. [27] identified a 42-kb fMyh super-enhancer (fMyh-SE) region that interacts with the fMyh promoter through 3D chromatin looping. However, the mechanisms by which transcription factors regulate the fine-tuned expression of each fMyh gene within myofibers via this enhancer region remain largely understudied. Our previous study was the first to successfully identify the large Maf transcription factor family (hereafter referred to as large Mafs in mice and large MAFs in humans) as a principal regulator of type IIb myofibers [28]. Although four large Mafs—*Mafa*, *Mafb*, *Maf*, and *Nrl*—have been identified in mammals, only *Mafa*, *Mafb*, and *Maf* are expressed in the skeletal muscle of mice and humans [28]. Furthermore, single deletion of *Mafa*, *Mafb*, or *Maf* in skeletal muscle does not affect the proportion of myofiber types. However, deletion of all three large Mafs in skeletal muscle leads to an almost complete loss of type IIb myofibers. This increases endurance capacity and reduces muscle force in mice [28]. Conversely, overexpression of each large Maf induced type IIb myofibers in the soleus muscle by binding to the Maf recognition element (MARE) located − 270 bp upstream of the transcription start site

of element *Myh4* in adult mice. These findings indicate that large Mafs are a potent and specific regulator of type IIb myofiber determination in mice [28]. However, their role in the skeletal muscle of larger animals, including humans, remains completely unknown. Moreover, the induction of fast-glycolytic type IIb myofibers—long lost in human skeletal muscle—through the manipulation of large MAFs remains a major scientific challenge.

The present study is the first report of the robust and specific expression of *MYH4*, a gene corresponding to type IIb fibers that is typically not expressed at the mRNA or protein level in humans. Overexpression of large MAFs increased the expression of this gene by 100- to 1000-fold in human and bovine skeletal muscle cells. Importantly, MYH4 was translated in human myotubes and detected via LC-MS/MS analysis. Furthermore, overexpression of large MAFs profoundly alters the expression of genes associated with glycolytic metabolism, thereby enhancing glycolytic activity in human skeletal muscle cells. Analysis of human muscle biopsy samples also revealed a positive correlation between *MAFA* and *MAF* expression and the proportion of fast-twitch myofibers in human skeletal muscle. Furthermore, *MAFA* and *MAF* expression was positively correlated with *MYH4* expression in human skeletal muscles, with the expression of these genes elevated in power-trained individuals. These findings suggest that large MAFs may unlock latent potential for the development of type IIb myofibers in humans.

Methods

Human iPS cloning and generation of muscle stem cells

The healthy donor-derived human pluripotent stem cell (hiPSC) clone 414C2 [29] was used to harvest iPSC-derived muscle stem cells (iMuSCs) after myogenic differentiation. Myogenic induction of hiPSCs was performed as previously described to obtain iMuSCs [30]. Briefly, undifferentiated hiPSCs were plated onto a 6-well plate coated with perlecan-binding laminin 421E8 fragments (p421E8) in StemFit AK02N (Ajinomoto) and 10 μM Y-27,632 (Nacalai) at 5×10^3 cells/well. After three days, the medium was replaced with CDMi supplemented with 10 μM CHIR99021 (CHIR, Wako) and 5 μM SB431542 (SB, Wako). CDMi is composed of IMDM (Wako) and Ham's F-12 medium (Wako) (ratio, 1:1) supplemented with 1% bovine serum albumin (BSA) (Sigma-Aldrich, Burlington, MA, USA), 1% penicillin-streptomycin mixed solution (Nacalai), 1% CD lipid concentrate (Thermo Fisher Scientific, Waltham, MA, USA), 1% insulin-transferrin selenium (Thermo Fisher Scientific), and 450 μM 1-thioglycerol (Sigma-Aldrich).

After seven days of differentiation, the cells were dissociated with Accutase (Nacalai) and plated onto a p421E8-coated 6-well plate (4.5×10^5 cells/well) in CDMi medium supplemented with 10 μM CHIR, 5 μM SB, and 10 μM Y-27,632. On differentiation day 14, the cells were dissociated with Accutase and placed onto an iMatrix-511 (Nippi)-coated 6-well plate (8×10^5 cells/well) in CDMi medium supplemented with 10 μM Y-27,632. The medium was replaced with serum-free culture medium (SF-O3; Sanko Junyaku) supplemented with 0.2% BSA, 200 μM 2-mercaptoethanol (2-ME), 10 ng/mL IGF-1 (PeproTech), 10 ng/mL recombinant human bFGF (Oriental Yeast), and 10 ng/mL recombinant human HGF (PeproTech) after three days. The medium was changed twice a week until day 38 of differentiation. On differentiation day 38, it was replaced with 2% horse serum (HS, Sigma-Aldrich) in DMEM (Nacalai) supplemented with 200 μM 2-ME (Nacalai), 10 ng/mL IGF-1, 5 μM SB, 0.5% penicillin-streptomycin mixed solution (Nacalai), and 2 mM L-glutamine (Nacalai). Thereafter, the medium was changed every 2–3 days, and the cells were cultured in the medium until weeks 11–12 of differentiation.

Isolation of iMuSCs through flow cytometric sorting

The cells were harvested for flow cytometric sorting after 11–12 weeks of differentiation [31]. Briefly, cells were dissociated with a Collagenase mix solution at 37 °C for 7 min. The collagenase mix solution is composed of DMEM supplemented with 0.05% Collagenase H (Meiji Seika Pharma) and 0.5% Collagenase G (Meiji Seika Pharma). Accutase was added to the solution and incubated at 37 °C for 10 min. The solution was subsequently neutralized with DMEM supplemented with 10% HS and centrifuged at 380 × *g* for 7 min at 4 °C. Next, the supernatant was removed. Cells were then resuspended in DMEM supplemented with 10% HS and filtered through a 40-μm cell strainer (Corning). Density gradient centrifugation was performed using Optiprep (Serumwerk Bernburg) in DMEM supplemented with 10% HS (ρ = 1.11 g/mL) according to the manufacturer's instructions to remove debris and dead cells. The fraction of living cells was resuspended in HBSS (Thermo Fisher Scientific) and 1% BSA before incubation with an APC-conjugated anti-CDH13 antibody (5×10^6 cells/mL) on ice for 15 min [32]. Flow cytometry was performed using Aria II (BD) in accordance with the manufacturer's instructions. Gating of the CDH-13-positive fraction was determined using unstained cells as the baseline control. After sorting the CDH-13-positive cells, the suspension was centrifuged at 780 × *g* for 10 min at 4 °C. The supernatant was removed, and the 2×10^5 sorted cells were cryopreserved in 200 μL Bambanker (NIPPON Genetics).

Re-culture and myogenic differentiation of sorted iMuSCs

Frozen sorted cells were rapidly thawed in a water bath at 37 °C. They were then suspended in a growth medium containing 39% DMEM (Gibco), 39% Ham's F12, 20%

FBS (Gibco), and 1% UltroserG (Pall Life Sciences). Next, the cells were centrifuged at 400 × *g* for 10 min at 4°C, as described previously [33, 34]. After removal of the supernatant, the cells were resuspended in a growth medium and plated on to an iMatrix-coated (nippi) 12-well plate (2×10^4 cells/well). The medium was replaced with a differentiation medium containing 2% HS in DMEM after three days. Thereafter, the medium was changed every 2 days until analysis. The growth and differentiation media were supplemented with 1% penicillin-streptomycin.

Preparation and culture of primary bovine muscle stem cells

The thoracic longissimus muscle was excised from a 22-month-old Holstein cow. Primary bovine muscle stem cells were isolated as described previously, with some minor modifications [35, 36]. Connective tissue, blood vessels, and fat tissue were removed from isolated muscle tissue under dissection microscopy. Minced muscle pieces were treated with 0.2% collagenase type II (Worthington Biochemical Corporation) in HBSS (Thermo Fisher) for 30–40 min at 37 °C. Muscle slurry was homogenized with an 18G needle passing through 10 times and subsequently incubated at 37 °C for another 10 min. Debris was filtrated through 100-μm and 40-μm cell strainers (Corning Japan KK). The obtained cells were cultured on non-coated dishes in 20% FBS (Biowest) in F10 (Thermo Fisher) supplemented with 2.5 ng/mL bFGF (Nacalai Tesque, Inc.) for 60 min. Next, a non-adherent fraction was collected as primary bovine MuSCs and cultured on collagen-coated dishes (AGC Techno Glass Co., Ltd.) for expansion. Cells with a few passages were cryopreserved and used for the experiments. Enrichment of primary bovine MuSCs and myotubes were confirmed through immunostaining with an antibody against sarcomeric-α-actinin, which is specifically expressed in skeletal muscles. The cells generated multinucleated myotubes after myogenic differentiation. In addition, > 50% of the cultured cells were positive for sarcomeric-α-actinin, which is specifically expressed in skeletal muscle cells.

Frozen bovine cells were rapidly thawed in a water bath at 37 °C and followed the same protocol as that for iMuSCs. Briefly, bovine cells were resuspended in growth medium and plated on to an iMatrix-coated (nippi) 12-well plate (2×10^4 cells/well). The medium was replaced with a differentiation medium containing 2% HS in DMEM after two days. Thereafter, the medium was changed every 2 days until analysis. The growth and differentiation media were supplemented with 1% penicillin-streptomycin.

Overexpression of Adenovirus-mediated large MAFs

The following adenoviral vectors were used to overexpress the large MAF transcription factor family in human iMuSCs and primary bovine MuSCs: pAV[Exp]-mCherry-CMV > hMAFA, pAV[Exp]-mCherry-CMV > hMAFB, and pAV[Exp]-mCherry-CMV > hMAF. pAV[Exp]-mCherry-CMV was used for control. All vectors were constructed and packaged by VectorBuilder Inc. (Chicago, IL, USA), with vector IDs as follows: VB010000-9300kfr (mCherry), VB900139-7528hhe (hMAFA), VB900139-7526uvc (hMAFB), and VB900139-7527axe (hMAF). The myotubes were incubated with adenovirus at a multiplicity of infection of 250 in differentiation medium for 48 h at two days post-differentiation of human iMuSCs or primary bovine MuSCs. The medium was then replaced with fresh differentiation medium without adenovirus. The myotubes were used for subsequent experiments at four days post-infection.

Immunofluorescence

Cultured cells were washed twice with PBS after removing the media and fixed with 4% paraformaldehyde for 15 min. The cells were permeabilized and blocked using 5% goat serum in 0.1% Triton PBS for 1 h at room temperature and subsequently washed thrice with PBS. The cultured cells were incubated with primary antibodies at 4 °C overnight. All immunostained samples were visualized using appropriate Alexa Fluor conjugated secondary antibodies (Thermo Fisher Scientific) for 1 h. Primary antibodies against RFP (600-401-379; Rockland), α-actinin (A7811; Sigma-Aldrich) were used. Moreover, secondary antibodies conjugated with Alexa Fluor-488, Alexa Fluor-555, and Alexa Fluor-647 were used.

Analysis of actively translated mRNA in human myotubes using AHA-mediated ribosomal isolation

The active ribosome was isolated with the AHARIBO RNA system (Immagina) as described previously [37] to analyze MYH4 mRNA translation in human myotubes. Briefly, adenovirus-infected human myotubes were washed once with PBS and treated for 40 min with methionine-free growth medium (Thermo Fisher Scientific) supplemented with 2% FBS and 0.8 mM l-leucine to deplete methionine reserves. After 40 min, 10 μL of AHA reagent was added to the medium. The cells were then incubated at 37 °C for 5 min, following the addition of 2.6 μL sBlock for 5 min at 37 °C. Next, they were placed on ice and washed once with 1 mL of cold PBS. PBS was carefully removed with a pipette, and cells were lysed with 45 μL of cold lysis buffer using a cell scraper. The cell lysate was transferred to a 1.5-mL microcentrifuge tube, and cell debris was pelleted through centrifugation at 20,000 × *g* for 5 min at 4 °C. The supernatant was transferred to a new tube and kept on ice for 20 min.

Absorbance was measured by NanoDrop at 260 nm, with lysis buffer as blank subtraction.

Two absorbance units (AU) of the sample was transferred to a new tube, and the volume was adjusted to 100 µL with freshly prepared SWB buffer to capture active ribosomal complexes. To this, 100 µL of sBeads was added, and the mixture was incubated for 60 min at 4 °C on a rotating wheel. Next, the supernatant was removed, and the beads were washed twice with WSS buffer. The beads were resuspended in 200 µL of SWB buffer. RNA was then extracted from the resuspended SWB buffer containing the beads. The extracted RNA concentration was measured at 260 nm using a NanoDrop spectrophotometer, and cDNA was subsequently synthesized.

Quantitative analysis of transcripts using reverse transcription PCR

Total RNA was extracted from human and bovine myotubes using TRIzol reagent (Life Technologies) according to the manufacturer's instructions. RNA (500 ng) or 340 ng of active ribosome-associated RNA was reverse transcribed using either the ReverTra Ace Kit with a genomic DNA remover (Toyobo, Osaka, Japan) or the QuantiTect Reverse Transcription Kit (Qiagen) for cDNA synthesis. Quantitative PCR was performed using the THUNDERBIRD SYBR qPCR system (Toyobo, Osaka, Japan) on a TP850 Thermal Cycler Dice Real-Time System (Takara Bio, Kusatsu, Japan). Primer sequences are listed in Supplementary Table 1. Transcription levels were normalized to the TATA-box-binding protein (TBP) transcript levels for each sample.

RNAscope

Adenovirus-infected human myotubes were fixed in 4% paraformaldehyde for 15 min to visualize MYH4 transcripts. Fixed cells were processed using the RNAscope Multiplex Fluorescent V2 Assay (323270; Advanced Cell Diagnostics), with MYH4 transcripts hybridized to Hs-MYH4-C1 probes (1583381-C1, ADC). Briefly, fixed cells were washed twice with PBS before incubation for 10 min in hydrogen peroxide solution. Cells were then treated with protease III and diluted 1:15 in PBS for 10 min. Next, they were washed twice and hybridized with the Hs-MYH4-C1 probe for 2 h at 40 °C. MYH4 transcripts were visualized using the TSA Vivid Fluorophore Kit 520 (R&D Systems) according to the manufacturer's instructions. Cells were washed twice in PBS, and immunofluorescence analysis was performed using antibodies against α-actinin and RFP, as described above. Nuclei were counterstained with DAPI.

RNA-seq analysis of human iMuSC-derived myotubes

Total RNA was extracted from human myotubes on day 4 of infection using TRIzol reagent (Thermo Fisher Scientific). The RNA sequencing (RNA-seq) library was prepared using the NEBNext Ultra Directional RNA Library Prep Kit (New England Biolabs, Ipswich, MA, USA) after ribosomal RNA (rRNA) depletion (NEBNext rRNA Depletion Kit; New England Biolabs). Paired-end (2 × 36 bases) sequencing was performed using the NextSeq500 platform (Illumina, San Diego, CA, USA). FASTQ files were imported to the CLC Genomics Workbench (Version 10.1.1; Qiagen, Hilden, Germany). Sequence reads were then mapped to the human reference genome (hg19). Gene expression was calculated as total read counts normalized by transcripts per million. Genes with zero counts in any sample were excluded, and differential expression was analyzed using the Empirical Analysis of DGE tool (edgeR test) in the CLC Main Workbench (Version 22.0; Qiagen). Differentially expressed genes (DEGs) were extracted among conditions (pAV-mCherry vs. pAV-MAFA vs. pAV-MAFB vs. pAV-MAF) with a false discovery rate–corrected $P < 0.05$. The DAVID Bioinformatics Resources 6.8 [38] was used for GO analysis, with P-value < 0.05.

Seahorse XF Glycolysis stress test

iMuSCs were seeded in XFe 24-well plates (Seahorse Bioscience, North Billerica, MA, USA) at a density of 1×10^4 cells/well. Adenoviral infection was performed on iMuSCs after 2 days of differentiation in differentiation medium (DM). The extracellular acidification rate (ECAR) was measured using a Seahorse XFe24 analyzer (Seahorse Bioscience) four days after infection. For the glycolysis stress test, glucose, oligomycin, and 2-deoxyglucose (2-DG) were sequentially added to the wells at final concentrations of 10 mM, 1.0 µM, and 50 mM, respectively. Glucose serves as a substrate for glycolysis, whereas oligomycin inhibits mitochondrial ATP synthase, consequently increasing reliance on glycolysis for energy production. Finally, 2-DG, a competitive inhibitor of glucose, effectively shuts down glycolysis.

Single-nucleus RNA-seq analysis

Single-nucleus RNA-seq data were downloaded from the Human Muscle Ageing Cell Atlas database (https://db.cngb.org/cdcp/hlma/), and the Seurat pipeline was applied to this dataset. The Seurat objects underwent normalization, scaling, and dimensional reduction. Types I and II myonuclei were classified based on previous studies [16]. We used density plots generated through the Nebulosa package in our snRNA-seq analysis to assess the localization of large MAFs within myonuclei [39]. Expression levels of large MAFs and MYH genes were measured in clusters of type II-positive myonuclei. Gene

expression in the snRNA-seq data was illustrated using two approaches: first, by plotting the expression levels of the gene across all myonuclei from young (15–46 years old, $n = 8$) and old (74–99 years old, $n = 19$) individuals; and second, by comparing the gene expression levels within myonuclei aggregated for each individual, grouped into young and old categories.

Mass spectrometry

Human myotube samples (10 mg) were reduced, alkylated, and digested with trypsin/Lys-C using the iST kit (iST 8x, P.O.00001, PreOmics, Germany) according to the manufacturer's instructions. The samples were then evaporated to dryness *in vacuo* to obtain residues. These residues were dissolved in 10 mL of LC-LOAD buffer from the iST kit. Peptides (200 ng) were injected into nanoLC/ESLI-MS/MS systems [LC: ACQUITY UPLC M-Class system (Waters, MA, USA), MS: ZenoTOF7600 (Sciex)]. The peptide samples were subsequently separated using the nanoEase M/Z Peptide CSH C18 column (1.7 mm, 0.075 3 150 mm) (Waters) at a flow rate of 300 nL/min. Mobile phase A consisted of a 0.1% (v/v) solution of formic acid in water, whereas mobile phase B consisted of a 0.1% (v/v) solution of formic acid in acetonitrile. The linear gradient conditions were as follows: 0–17 min: 2% solvent B, 17–125 min: 30% B, 126–127 min: 40% B, 127–132 min: 80% B, 132–133 min: 90% B, 133–153 min: 90% B, 153–154 min: 2% B, 154–180 min: 2% B. The mass spectrometer was operated in a Zeno SWATH acquisition scheme with 100 variable-size windows, and 25 ms accumulation time was used. The Zeno SWATH raw MS data were processed using DIA-NN 1.8.1 [40], available on github (DIA-NN github repository).

The human spectral libraries were generated from the human spectral library and human UniProt database (id UP000005640, reviewed, canonical). The DIA-NN search parameters were as follows: experimental data search enzyme, trypsin; missed cleavage sites, 1; peptide length range, 7–30; precursor mass charge range, 1–4; precursor m/z range, 300–1800; fragment ion m/z range, 200–1800; and static modification, cysteine carbamidomethylation. The protein identification threshold was set at < 1% for both peptide and protein FDR. Each peptide assigned to MYH4 was verified through a BLAST search, and peptides specific to MYH4 were counted. The newly acquired mass spectrometry proteomic data have been deposited to the Proteome Xchange Consortium via jPOSTrepo [41] with the dataset identifier JPST003487.

Comparison of gene expression patterns across multiple animal species

Bgee v15.2.0 was used [42] to compare MYH4 and large MAF expression scores across animal species. Expression scores are based on non-parametric statistics, where conditions are ranked based on the gene expression levels. These ranks are then normalized across conditions, genes, and data types, and transformed into an expression score ranging from 0 (low expression) to 100 (high expression). These non-parametric statistics enable quantitative comparison of gene expression across species and conditions without requiring batch-correction procedures. The anatomical entities included in the analysis were skeletal muscle tissue (opossum, dog, and cow), quadricep muscle (mouse, rat, and human), and general muscle tissue (horse).

Motif enrichment analysis

The presence of MAF recognition element sites in the promoter regions of genes were predicted through the Find Individual Motif Occurrences (FIMO) algorithm of the MEME Suite [43], using the position weight matrix available from JASPAR (https://jaspar.genereg.net/). This analysis was run from 3 kb upstream to 3 kb downstream of the *Myh4* transcriptional start in mice, rats, opposums, humans, dogs, cows, and horses.

Study participants

The Russian part of the study was approved by the Ethics Committee of the Federal Research and Clinical Center of Physical–Chemical Medicine of the Federal Medical and Biological Agency of Russia (protocol no. 2017/04). The Finnish part of the study was approved by the Hospital District of Helsinki and Uusimaa (these data were used with permission; Database of Genotypes and Phenotypes Study Accession: phs001048.v2.p1). Written informed consent was obtained from each participant. The study complied with the Declaration of Helsinki and ethical standards for sport and exercise science research.

The Russian gene expression study (analysis of MAF gene expression in m. vastus lateralis) involved 24 men (mean age ± SD: 32.7 ± 8.9 years; mean height: 180.8 ± 6.8 cm; mean body mass: 80.1 ± 11.6 kg; mean percentage of fast-twitch muscle fibers: 50.3 ± 21.3%; mean percentage of slow-twitch muscle fibers: 52.7 ± 21.6%; cross-sectional area (CSA) of fast-twitch muscle fibers: 5934 ± 1833 μm^2; CSA of slow-twitch muscle fibers: 5545 ± 1197 μm^2). Outliers were identified using Grubbs' test (Alpha = 0.05) in GraphPad Prism; three participants with outlying MYH4 expression levels were excluded from the analysis.

The Finnish study involved 291 individuals (166 men, mean age 59.5 ± 8.1 years; mean height: 176.7 ± 6.7 cm; mean body mass: 87.3 ± 15.1 kg; mean percentage of fast-twitch muscle fibers: 58.9 ± 14.7%; mean percentage of slow-twitch muscle fibers: 41.1 ± 14.7%; 125 women, mean age: 60.3 ± 8.1 years; mean height: 162.8 ± 5.6 cm; mean body mass: 71.8 ± 9.8 kg; mean percentage of fast-twitch muscle fibers: 49.9 ± 13.3%; mean percentage

of slow-twitch muscle fibers: 50.1 ± 13.3%) from the FUSION study, as previously described [44].

Evaluation of muscle fiber composition in human muscle biopsy samples

Vastus lateralis samples of Russian participants were obtained from the left leg using the modified Bergström needle procedure, with aspiration under local anesthesia using a 2% lidocaine solution. Samples were frozen in liquid nitrogen and stored at -80 °C before analysis. Serial cross-Sect. (7 µm) were obtained from frozen samples using an ultratom (Leica Microsystems, Wetzlar, Germany). Sections were then thaw-mounted on Polysine glass slides, maintained at room temperature (RT) for 15 min and incubated in PBS (3 × 5 min). The sections were then incubated at RT in primary antibodies against slow or fast isoforms of the myosin heavy chains (M8421, 1:5000; M4276; 1:600, respectively; Sigma-Aldrich) for 1 h and incubated in PBS (3 × 5 min). Next, the sections were incubated at RT in secondary antibodies conjugated with FITC (F0257; 1:100; Sigma-Aldrich) for 1 h. Antibodies were removed, and the sections were washed in PBS (3 × 5 min), placed in mounting media, and covered with a cover slip. Images were captured with a fluorescent microscope (Eclipse Ti-U; Nikon, Tokyo, Japan). All analyzed images contained 334 ± 14 fibers. The ratio of the number of stained fibers to the total fiber number was calculated. Fibers stained in serial sections with antibodies against slow and fast isoforms were considered hybrid fibers. The CSAs of fast- and slow-twitch muscle fibers were evaluated using ImageJ software (NIH, USA).

Muscle fiber composition in 287 Finnish individuals was estimated based on the expression of MYH1, MYH2, MYH7, Ca^{2+} ATPase A1, and Ca^{2+} ATPase A2 genes, as previously described [44]. Muscle samples were obtained from the vastus lateralis using a conchotome, under local anesthesia with 20 $mg{\cdot}ml^{-1}$ lidocaine hydrochloride without epinephrine.

RNA-seq analysis of human muscle biopsy samples

Russian participants were asked not to train for one day before biopsy of the vastus lateralis of the left leg to analyze their gene expression profiles at the resting state. The RNeasy Mini Fibrous Tissue Kit (Qiagen) was used to isolate RNA from 24 muscle tissue samples. Frozen tissue samples were placed in a box submerged in liquid nitrogen. Each frozen sample was transferred onto a sterile Petri dish placed on a frozen plastic ice pack. A piece of tissue with a weight of 10 mg was separated with a sterile scalpel and immediately placed in a 2 mL safe-lock microcentrifuge tube containing 300 µL of lysis buffer and one sterile stainless-steel bead with a diameter of 4 mm. Samples were homogenized using the TissueLyser II system (Qiagen) and shaken twice for 2 min at 25 Hz. RNA samples were isolated according to the manufacturer's guidelines. RNA concentration was measured using the Qubit spectrophotometer (Thermo Fisher Scientific). RNA quality was assessed using the BioAnalyzer electrophoresis system and BioAnalyzer RNA Nano assay (Agilent Technologies, Santa Clara, CA, USA). The RNA integrity number (RIN) was calculated for each RNA sample. Only RNA samples with RIN > 7 were included in the study. Samples were stored at − 80 °C until sequencing libraries were prepared. Total RNA samples were treated with DNase I using the Turbo DNA-free Kit (Thermo Fisher Scientific) according to the manufacturer's instructions. Libraries for RNA sequencing were prepared using the Illumina NEBNext Ultra II Directional RNA Library Prep Kit with the NEBNext rRNA Depletion Module (New England Biolabs). RNA libraries were sequenced on the Illumina HiSeq system with 250 cycles. Sequenced reads were pseudoaligned to the hg38 gencode (v37) transcriptome using kallisto v0.48.0 [45] with default settings. Gene-level expression abundances were calculated using the tximport Bioconductor package [46]. Expression of large MAFs and MYH genes is presented in transcripts per million (TPM).

RNA isolation and sequencing in the Finnish samples was performed using strand-specific mRNA-seq, as previously described [44]. Using the basic GENCODE v19 annotations [47], we counted fragments mapping to each gene using htseq-count v0.5.4 [48] and quantified gene expression as TPM.

Statistical analysis

Data are presented as the mean ± SEM, as indicated in the Figure legends. Statistical significance was determined using GraphPad Prism software (v10.4.0) through Student's *t*-test or one-way analysis of variance with Tukey's test. $^{*}P < 0.05$, $^{**}P < 0.01$, $^{***}P < 0.001$; ns, not significant.

Results

Large MAFs as conserved regulators of MYH4 across species and human aging

We analyzed the expression levels of *MYH4* (human), *Myh4* (mouse), and their orthologs in other species, as well as those of large MAF genes (*MAFA*, *MAFB*, and *MAF*) across various animal species using the Bgee database [42] to investigate why large mammals lack type IIb myofibers and the corresponding *MYH4* gene. The expression score of *MYH4*/*Myh4* and the combined mRNA expression scores of *MAFA*, *MAFB*, and *MAF* are shown in Fig. 1A. A positive correlation was observed between large MAF mRNA expression and *MYH4*/*Myh4* mRNA expression across species. Small animals such as mice, rats, and opossums exhibited relatively higher expression levels of large *MAFs*, whereas larger mammals, including horses, cattle, and dogs tended to show

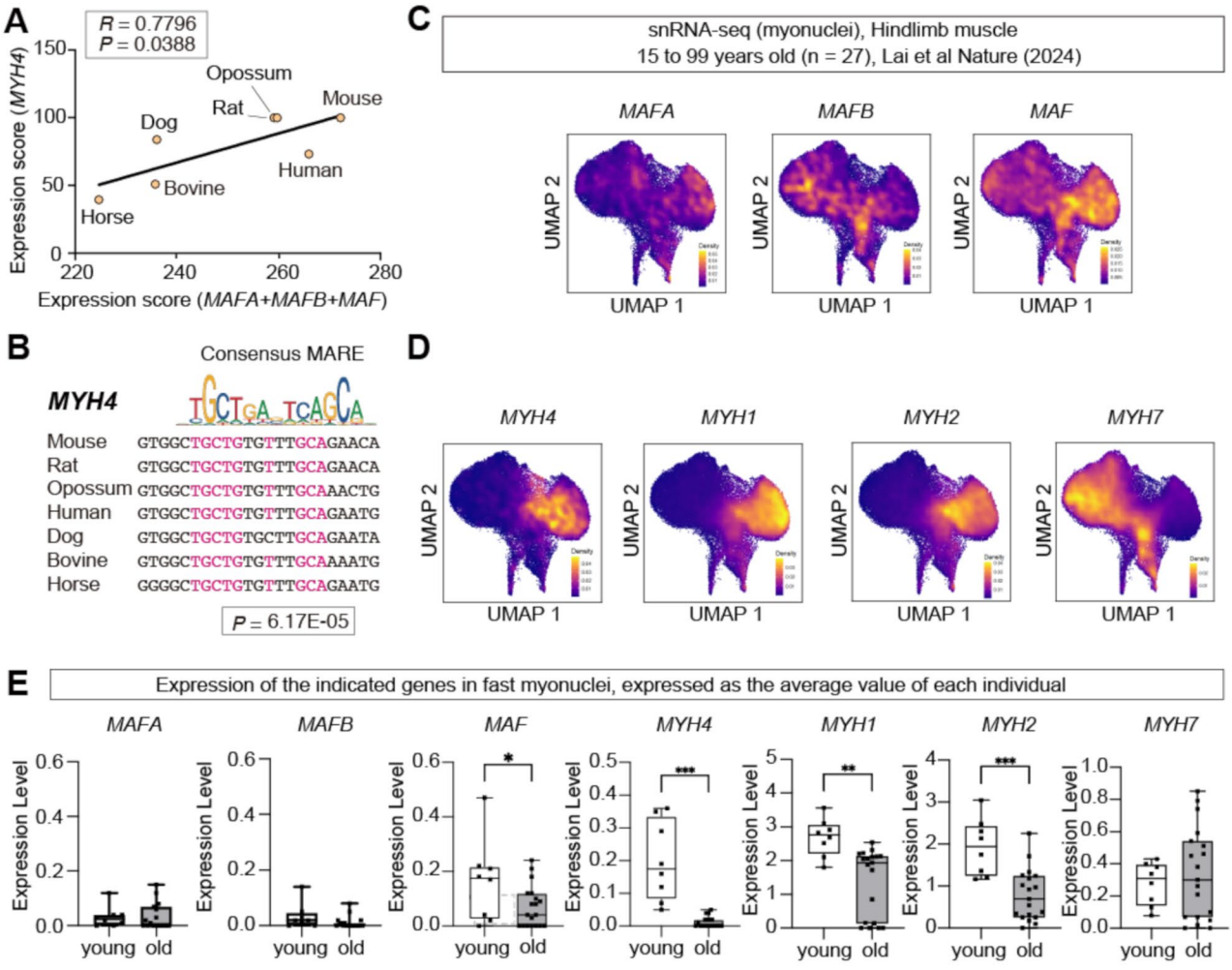

Fig. 1 MYH4 expression fluctuates in response to large MAF expression. (**A**) Correlation between the expression of large MAFs (*MAFA*, *MAFB*, and *MAF*) and *MYH4* across multiple animal species. (**B**) Presence of MARE-like sequences in the promoter region of *Myh4* across multiple animal species. (**C**) Visualization of *MAFA*, *MAFB*, and *MAF* expression using UMAP, as derived from single-nucleus RNA sequencing (snRNA-seq) of human hindlimb muscle samples from individuals aged 15–99 years ($n = 27$). Data sourced from Lai et al., *Nature* (2024). (**D**) Visualization of *MYH4*, *MYH1*, *MYH2*, and *MYH7* expression using UMAP, as derived from snRNA-seq of human hindlimb muscle samples from individuals aged 15–99 years ($n = 27$). Data sourced from Lai et al., *Nature* (2024). (**E**) Average expression levels of *MAFA*, *MAFB*, *MAF*, *MYH4*, *MYH1*, *MYH2*, and *MYH7* in myonuclei, expressed as the mean value for each individual in the respective age groups (young: 15–46 years, $n = 8$; old: 74–99 years, $n = 19$). *P* values were calculated using a two-sided Pearson correlation test (**A**) and an unpaired two-tailed *t*-test (**E**); $^{*}P < 0.05$, $^{**}P < 0.01$, $^{***}P < 0.001$, $^{****}P < 0.0001$, R; Pearson correlation coefficient

lower expression levels. Although these trends suggest a potential species-level association between large *MAF* expression and *MYH4*, the anatomical sources and muscle types are not strictly matched across species. Moreover, the relatively high expression of large MAFs in humans—despite low *MYH4* expression—suggests that additional regulatory mechanisms constrain *MYH4* expression in human skeletal muscle. Therefore, these data should be interpreted with caution. Nonetheless, the observed pattern indicates that large MAFs may contribute to the evolutionary regulation of type IIb myofiber abundance across diverse animal species.

Large MAFs directly induce type IIb myofibers via a MARE site within the *Myh4* promoter region in mice [28]. To determine whether this regulatory mechanism is also conserved in large mammals, we examined the *MYH4* promoter sequences across several species (Fig. 1B). The MARE sequence was highly conserved not only in small animals, such as rodents, but also in larger mammals, including humans, cattle, and horses (Fig. 1B). This conservation suggests that large *MAFs* retain the potential to regulate *MYH4* expression via the MARE in these species, even though *MYH4* is transcriptionally repressed in their skeletal muscle.

We subsequently analyzed single-nucleus RNA sequencing (snRNA-seq) data of human skeletal muscle [16] to evaluate the role of large MAFs. Although *MYH4* expression was minimal in human skeletal muscle, *MAFA*

and *MAF* were enriched in fast myonuclei expressing *MYH2*, *MYH1*, and *MYH4* (Fig. 1C, D). Although *MAFB* was also expressed in myonuclei, its expression was broadly distributed across myonuclei expressing both fast and slow *MYH* genes (Fig. 1C, D).

We compared snRNA-seq data from young individuals (15–46 years old) with those from elderly individuals (74–99 years old) to examine the effect of aging on the expression of these genes (Fig. 1E). Analysis of *MAFA*, *MAFB*, and *MAF* expression in fast myonuclei revealed a significant downregulation of *MAF* expression in older individuals (Fig. 1E). In contrast, the expression levels of *MAFA* and *MAFB* were comparable between young and older individuals. The expression of fast-type *MYH*, such as *MYH1*, *MYH2*, and *MYH4*, showed a substantial decline with aging (Fig. 1E). In contrast, *MYH7* expression did not differ significantly between older and younger individuals (Fig. 1E). These results suggest that large MAFs regulate fast myofiber gene expression in human skeletal muscle and highlight their physiological relevance in human aging.

Large MAFs specifically induce MYH4 expression in human skeletal muscle cells

To investigate whether large MAFs play a role in the induction of type IIb myofibers in humans, we overexpressed *MAFA*, *MAFB*, or *MAF* using adenoviral vectors in human skeletal muscle cells derived from previously established human iPS cells [32, 49]. Sorted induced muscle stem cells (iMuSCs) derived from iPS cells were differentiated for 2 days in DM before transduction with adenoviral particles expressing *MAFA*, *MAFB*, or *MAF* driven by the CMV promoter (Fig. 2A). An adenoviral vector expressing *mCherry* alone was used as control (CON) (Fig. 2A) No abnormalities were observed in myotubes overexpressing *MAFA*, *MAFB*, or *MAF* compared to the control myotubes following viral transduction (Fig. 2B). The infection efficiency, determined based on the percentage of mCherry-positive myotubes, was comparable across all groups (>90%) (Fig. 2B-C). Myotube width was unaffected by large MAF overexpression (Fig. 2D). Furthermore, *MAFA*, *MAFB*, and *MAF* were successfully overexpressed in human myotubes (Fig. 2E).

We further performed RNAscope fluorescent in situ hybridization to determine whether large MAFs induce *MYH4* expression. *MYH4* RNA puncta were barely detectable in control human myotubes overexpressing mCherry (Fig. 2F). However, *MYH4* puncta were clearly accumulated in all large MAF-overexpressing myotubes (Fig. 2F). We used qPCR analysis to further quantify the expression levels of *MYH4* and other *MYH* genes. Although *MYH4* expression in control myotubes was markedly low, it was elevated by approximately 100- to 1000-fold in large MAF-overexpressing myotubes compared to the controls (Fig. 2G-I). However, large MAFs did not increase—and, in some cases, reduced—the transcription levels of *MYH7*, *MYH2*, and *MYH1*. These findings demonstrate that the overexpression of large MAFs can specifically induce *MYH4* expression in human skeletal muscle cells.

We isolated primary bovine MuSCs and conducted adenoviral infection in bovine myotubes to further confirm that the mechanism underlying *MYH4* expression by large MAFs is conserved across large mammalian species (Fig. S1A). Bovine MuSCs formed multinucleated myotubes with well-defined sarcomere structures after 6 days of differentiation (Fig. S1B). After adenoviral infection, we performed qPCR analysis to evaluate *MYH4* and *MYH7* expression in bovine myotubes (Fig. S1C-H). *MYH4* was barely detectable in bovine myotubes expressing mCherry alone. However, the expression of its transcripts was substantially upregulated in all large MAF-overexpressing cells (Fig. S1C-E). Additionally, *MYH7* expression was significantly decreased in all large MAF-overexpressing bovine myotubes (Fig. S1F-H). Given the highly conserved MARE sites in the *MYH4* promoter across species, these findings demonstrate that large MAFs act as universal regulators of *MYH4* expression across mammalian species.

Human extraocular muscles exhibit detectable levels of *MYH4* mRNA but not the corresponding protein [24, 50]. This indicates two possibilities: insufficient *MYH4* mRNA levels or translational suppression of *MYH4* in human skeletal muscle. Thus, we investigated whether *MYH4* mRNA induced by large MAFs can be translated into protein. RNA bound to active ribosomes was extracted using the AHARIBO RNA system [37], and RT-qPCR was subsequently performed to assess the binding of *MYH4* mRNA to active ribosomes (Fig. 3A). We detected amplification of *MYH4* mRNA bound to active ribosomes in large MAF-overexpressing myotubes (Fig. 3B, C), whereas no *MYH4* amplification was observed in control myotubes (Fig. 3B, C). To further confirm the presence of MYH4, we conducted LC-MS/MS analysis in human myotubes overexpressing large MAFs (Fig. 3D). Human MAFA, MAFB, and MAF peptides were only observed in myotubes overexpressing *MAFA*, *MAFB*, and *MAF*, respectively (Fig. 3E-G). Furthermore, *MYH4*-specific peptides were detected in myotubes overexpressing *MAFB* and *MAF* but not in the control (Fig. 3H, I). MYH4 peptides were observed in only one sample of *MAFA*-overexpressing myotubes (Fig. 3H, I), which was consistent with mild *MAFA*-mediated induction of *MYH4* mRNA compared to *MAFB* and *MAF* (Fig. 2G). These findings provide the first functional evidence that *MYH4* expression can be actively induced through the overexpression of large MAF transcription factors in human skeletal muscle cells, revealing the

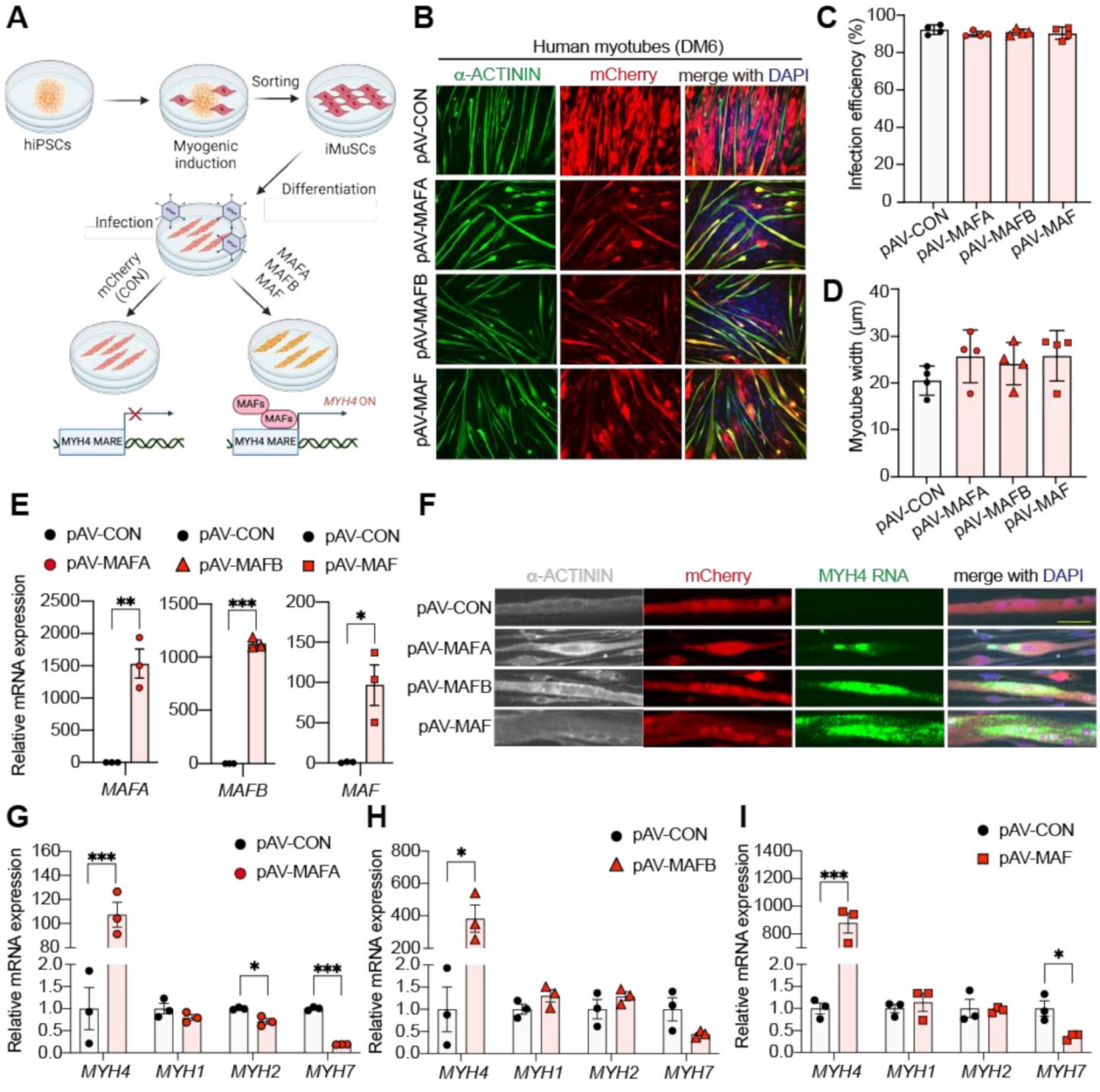

Fig. 2 Large MAFs can specifically induce MYH4 mRNA expression in human iPSC-derived myotubes. (**A**) A schematic diagram illustrating adenovirus-mediated overexpression of MAFA, MAFB, and MAF in human iPSC-derived myotubes. After myogenic induction, iMuSCs were purified using flow cytometry and cultured in growth medium for expansion. After two days of exposure to differentiation medium, human myotubes were treated with adenoviral particles expressing MAFA_mCherry (pAV-MAFA), MAFB_mCherry (pAV-MAFB), or MAF_mCherry (pAV-MAF). mCherry-only was used as the control (pAV-CON). Created in BioRender. Ryo, F. (2025) https://BioRender.com/r49s132. (**B**) Immunostaining of human myotubes transduced with pAV-CON, pAV-MAFA, pAV-MAFB, or pAV-MAF using antibodies against alpha-actinin (α-ACTININ, green) and mCherry (red). Nuclei were stained with DAPI (blue). (**C**) Quantification of infection efficiency for each adenoviral vector. The proportion of mCherry-positive cells within α-ACTININ-positive myotubes was calculated. In total, 91–105 myotubes were analyzed per experiment ($n = 4$). (**D**) Quantification of myotube width shown in panel (**B**). In total, 157–283 myotubes were analyzed per experiment ($n = 4$). (**E**) Relative mRNA expression levels of MAFA, MAFB, and MAF, as determined using RT-qPCR in human myotubes 4 days after adenovirus transduction ($n = 3$/group). (**F**) Detection of MYH4 mRNA in human myotubes transduced with pAV-CON, pAV-MAFA, pAV-MAFB, or pAV-MAF using RNAscope. Myotubes were visualized with an antibody against α-ACTININ (white) and mCherry (red) after hybridization. Nuclei were stained with DAPI (blue). Scale bar: 50 μm. (**G-I**) Relative mRNA expression levels of myosin heavy chain genes (*MYH1*, *MYH2*, *MYH4*, and *MYH7*), as determined using RT-qPCR in human myotubes 4 days after transduction with adenoviral vectors expressing MAFA (**G**), MAFB (**H**), or MAF (**I**). mCherry-only was used as the control (pAV-CON, $n = 3$/group). *P* values were calculated using Tukey's test (**C**, **D**) and Student's *t*-test (**E**, **G-I**); $^{*}P < 0.05$, $^{**}P < 0.01$, $^{***}P < 0.001$

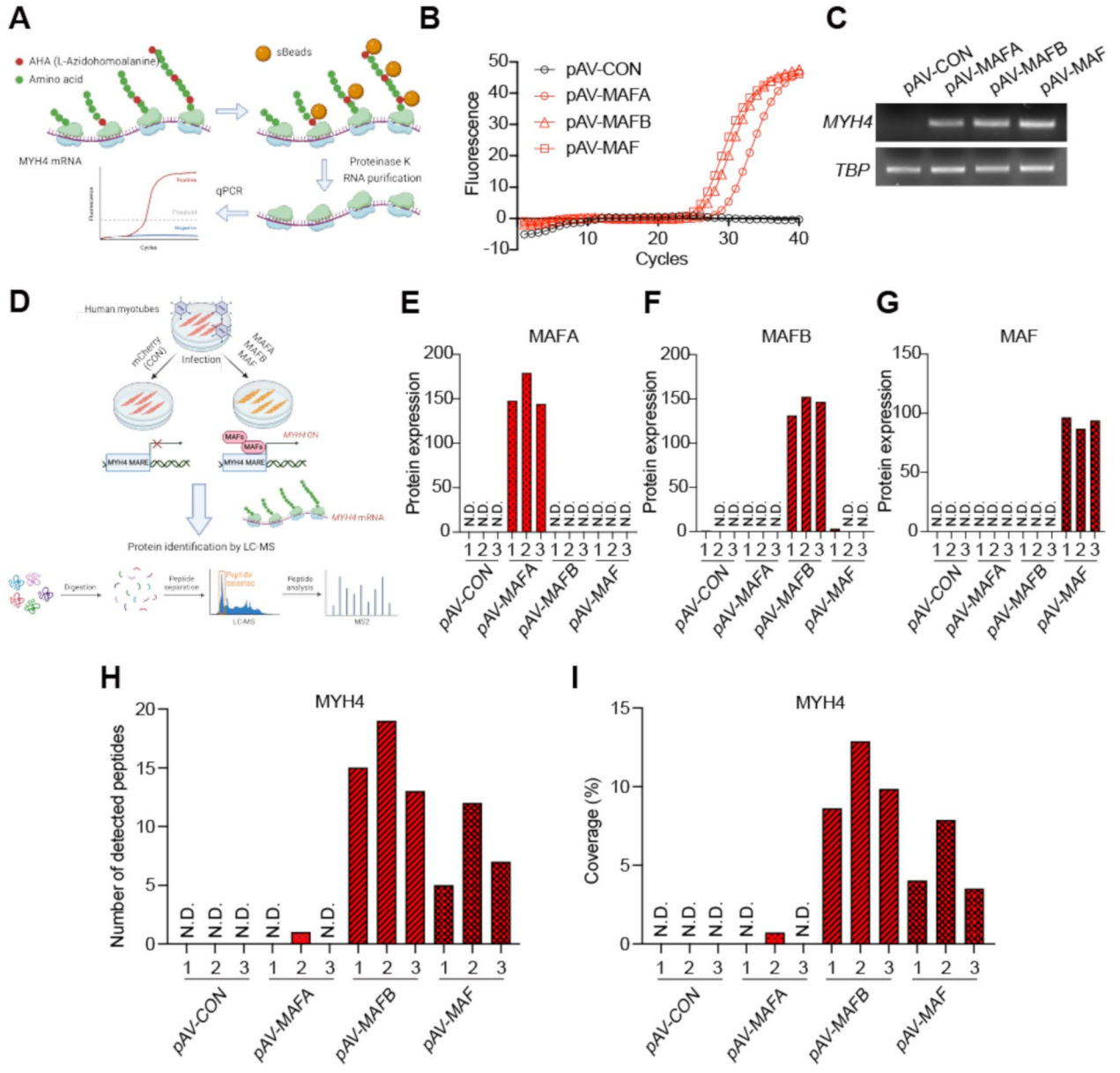

Fig. 3 MYH4 mRNA induced by large MAFs is translated into protein in human myotubes. (**A**) A schematic diagram illustrating the protocol for isolating active ribosomes to detect MYH4 mRNA translation in human myotubes following adenoviral overexpression of MAFA, MAFB, or MAF. Created in BioRender. Ryo, F. (2025) https://BioRender.com/g05y857. (**B**) The amplification curve of MYH4 mRNA bound to active ribosomes in human myotubes, as determined using RT-qPCR. (**C**) Gel electrophoresis of qPCR products corresponding to MYH4 and TBP mRNAs bound to active ribosomes, as analyzed in panel (**B**). (**D**) A schematic diagram illustrating the protocol for the detection of MYH4 using LC-MS/MS in human myotubes following adenoviral overexpression of MAFA, MAFB, or MAF. Created in BioRender. Ryo, F. (2025) https://BioRender.com/f96f475. (**E-G**) MAFA (E), MAFB (F), and MAF (G) expression in human myotubes following adenoviral overexpression of MAFA, MAFB, or MAF, as determined via LC-MS/MS. mCherry-only was used as the control (pAV-CON) ($n = 3$/group). N.D.; not detected. (**H**) The number of MYH4-specific peptides detected in human myotubes following adenoviral overexpression of MAFA, MAFB, or MAF, as determined using LC-MS/MS. mCherry-only was used as the control (pAV-CON, $n = 3$/group). N.D.; not detected. (**I**) Percent peptide coverage of MYH4 in LC-MS/MS analysis. Coverage is expressed as the percentage of the amino acid sequences detected via LC-MS/MS analysis

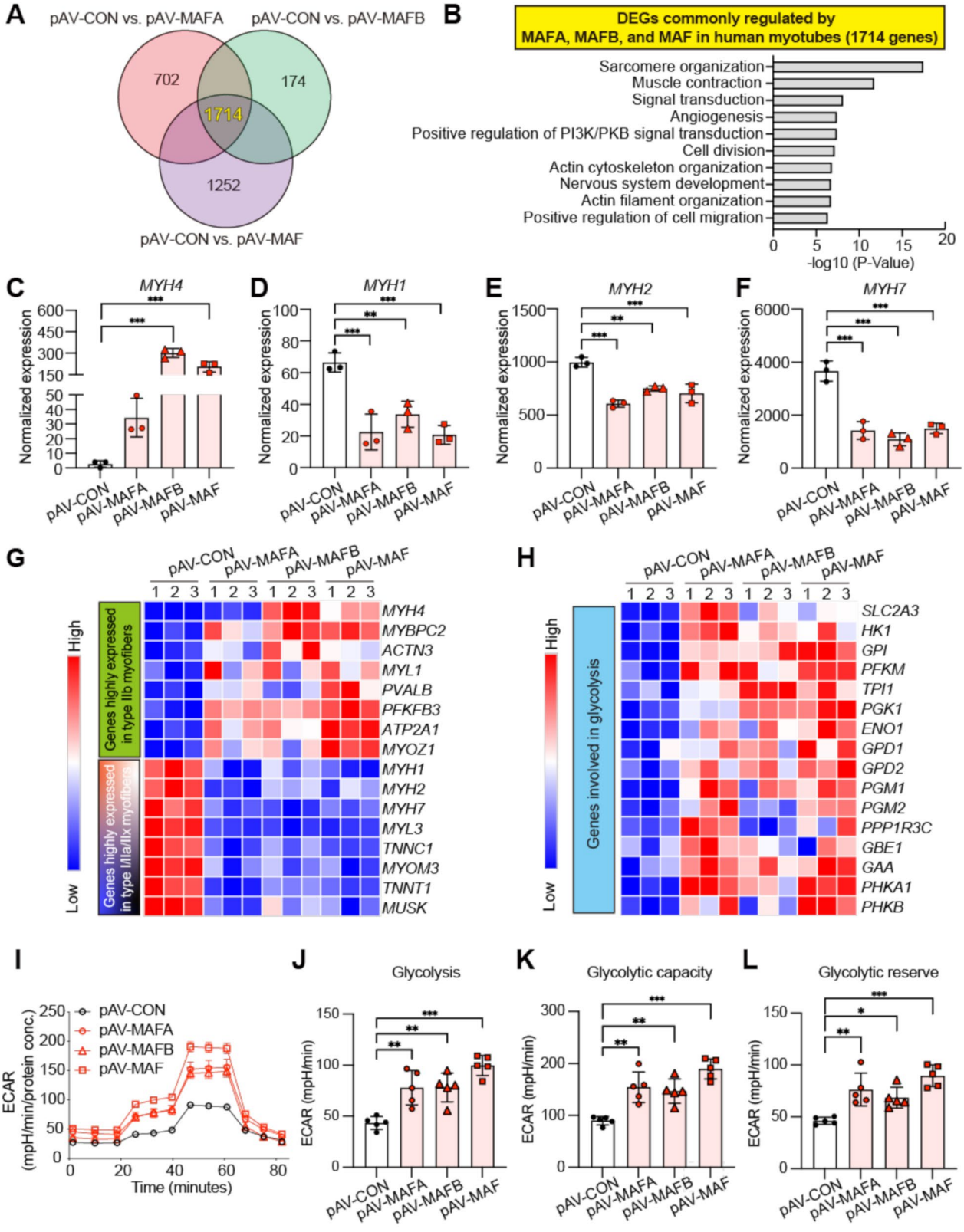

Fig. 4 (See legend on next page.)

(See figure on previous page.)

Fig. 4 Large MAFs specifically upregulate the expression of type IIb myofiber-associated and glycolytic genes, consequently enhancing glycolysis in human myotubes. (**A**) Venn diagrams showing the differentially expressed genes (DEGs) identified in comparisons between pAV-CON and pAV-MAFA (3,685 genes), pAV-CON and pAV-MAFB (2,289 genes), and pAV-CON and pAV-MAF (4,446 genes). In total, 1,714 DEGs were commonly altered by the overexpression of large MAFs. (**B**) Gene ontology (GO) analysis of the 1,714 commonly altered genes identified in panel (**A**). (**C-F**) RNA-seq analysis of MYH4, MYH1, MYH2, and MYH7 expression in human myotubes transduced with pAV-CON, pAV-MAFA, pAV-MAFB, or pAV-MAF ($n = 3$/group). (**G**) A heatmap visualizing the expression of type IIb myofiber-associated genes and other myofiber type-associated genes ($n = 3$/group). (**H**) A heatmap visualizing the expression of genes involved in glycolysis ($n = 3$/group). (**I**) Extracellular acidification rate (ECAR) in human myotubes transduced with pAV-CON, pAV-MAFA, pAV-MAFB, or pAV-MAF, as measured using the Seahorse XFe24 Analyzer ($n = 5$/group). (**J-L**) Glycolysis, glycolytic capacity, and glycolytic reserve calculated from the ECAR data shown in panel (**I**). *P* values were calculated using Tukey's test (**C-F**, **J-L**); $^{*}P < 0.05$, $^{**}P < 0.01$, $^{***}P < 0.001$, $^{****}P < 0.0001$

latent capacity of *MYH4* to be reactivated under defined regulatory conditions.

Large MAFs as key regulators of type IIb myofiber-specific and glycolytic gene programs in human skeletal muscle cells

In the present study, we extend our previous findings in mice [28] to humans and cattle, providing evidence that *MYH4* is directly controlled by large MAFs in these species. Although MYH4 is the most critical marker of type IIb myofibers, its expression alone is insufficient to define the formation of authentic type IIb myofibers. To investigate the extent to which large MAFs regulate genes beyond *MYH4*, including genes highly enriched in type IIb myofibers and those involved in glycolysis, we conducted a comprehensive RNA-seq analysis in human myotubes overexpressing *MAFA*, *MAFB*, or *MAF* using the adenoviral vectors described in Fig. 2A.

We observed robust transcriptional changes in myotubes overexpressing each large MAF, with 3,685 transcripts altered in *MAFA*-overexpressing myotubes (1,907 upregulated and 1,778 downregulated), 2,289 transcripts in *MAFB*-overexpressing myotubes (1,195 upregulated and 1,094 downregulated), and 4,446 transcripts in *MAF*-overexpressing myotubes (2,262 upregulated and 2,184 downregulated) compared to control myotubes (Fig. 4A).

The expression of 1,714 genes was commonly regulated across myotubes overexpressing large MAFs, including 845 and 869 genes with upregulated and downregulated expression, respectively (Fig. 4A). Gene ontology (GO) analysis of these DEGs revealed strong enrichment of pathways related to sarcomere organization and muscle contraction (Fig. 4B). Moreover, GO analysis of genes specifically altered by each large MAF in human myotubes suggested unique roles for each transcription factor. However, this may be unrelated to myofiber determination, as no significant enrichment for muscle-related GO terms was detected in these gene sets (Fig. S2A-C). The changes in the expression of adult *Myh* genes closely mirrored the RT-qPCR results shown in Fig. 2G–I. This confirms that *MYH4* expression was specifically and substantially upregulated by large MAFs (Fig. 4C). Its induction was more pronounced in *MAFB*- and *MAF*-overexpressing myotubes than in *MAFA*. Conversely, large MAFs suppressed *MYH7*, *MYH1*, and *MYH2* expression (Fig. 4D–F).

Consistent with the changes induced by large MAFs in sarcomere organization and muscle contraction (Fig. 4B), the expression of isoforms of contractile proteins enriched in type IIb muscles was markedly upregulated (e.g., *MYBPC2*, *ACTN3*, and *MYL1*) (Fig. 4G). In contrast, the expression of isoforms associated with type I, IIa, and IIx muscles (e.g., *TNNC1* and *TNNT1*) was downregulated (Fig. 4G). Analysis of genes associated with myofiber type transitions revealed that expression of the myocyte enhancer factor 2 (MEF2) family (*MEF2A*, *MEF2B*, and *MEF2C*), which promotes slow oxidative myofibers, was downregulated in large MAF-overexpressing myotubes compared to mCherry-overexpressing controls (Fig. S3A). Transcription factors associated with fast glycolytic muscle genes, including *SIX1*, *SIX4*, *TBX15*, *FNIP1*, *EYA1*, and *SMARCD3* [8, 51–55], were not notably induced by large MAFs in human myotubes (Fig. S3A). Although myotube width in human myotubes did not differ significantly among groups (Fig. 2D), the expression of genes involved in myogenesis, such as *MYOG* [56], was downregulated by large MAF overexpression (Fig. S3B).

Type IIb myofibers are further characterized by their high glycolytic gene expression. The loss of large Mafs affects not only fiber type composition but also metabolic profiles in mouse skeletal muscles [28, 57]. We sought to determine whether the overexpression of large MAFs elevated the expression of glycolytic genes [58] in human myotubes. RNA-seq analysis revealed significant upregulation of glycolytic gene expression in large MAF-overexpressing myotubes (Fig. 4H). Moreover, we confirmed the presence of MARE sites within the promoters of the glycolytic genes listed in Fig. 4H.

The profound transcriptional changes in glycolytic genes prompted further investigation into glycolytic activity in human myotubes upon large MAF overexpression. We measured the ECAR using the Agilent XF Seahorse technology to generate live-cell bioenergetic profiles. The overexpression of large MAFs significantly enhanced glycolytic rates, including glycolysis, glycolytic capacity, and glycolytic reserve, in large MAF-overexpressing human myotubes compared to controls (Fig. 4I-L). Our findings demonstrate that large MAFs broadly

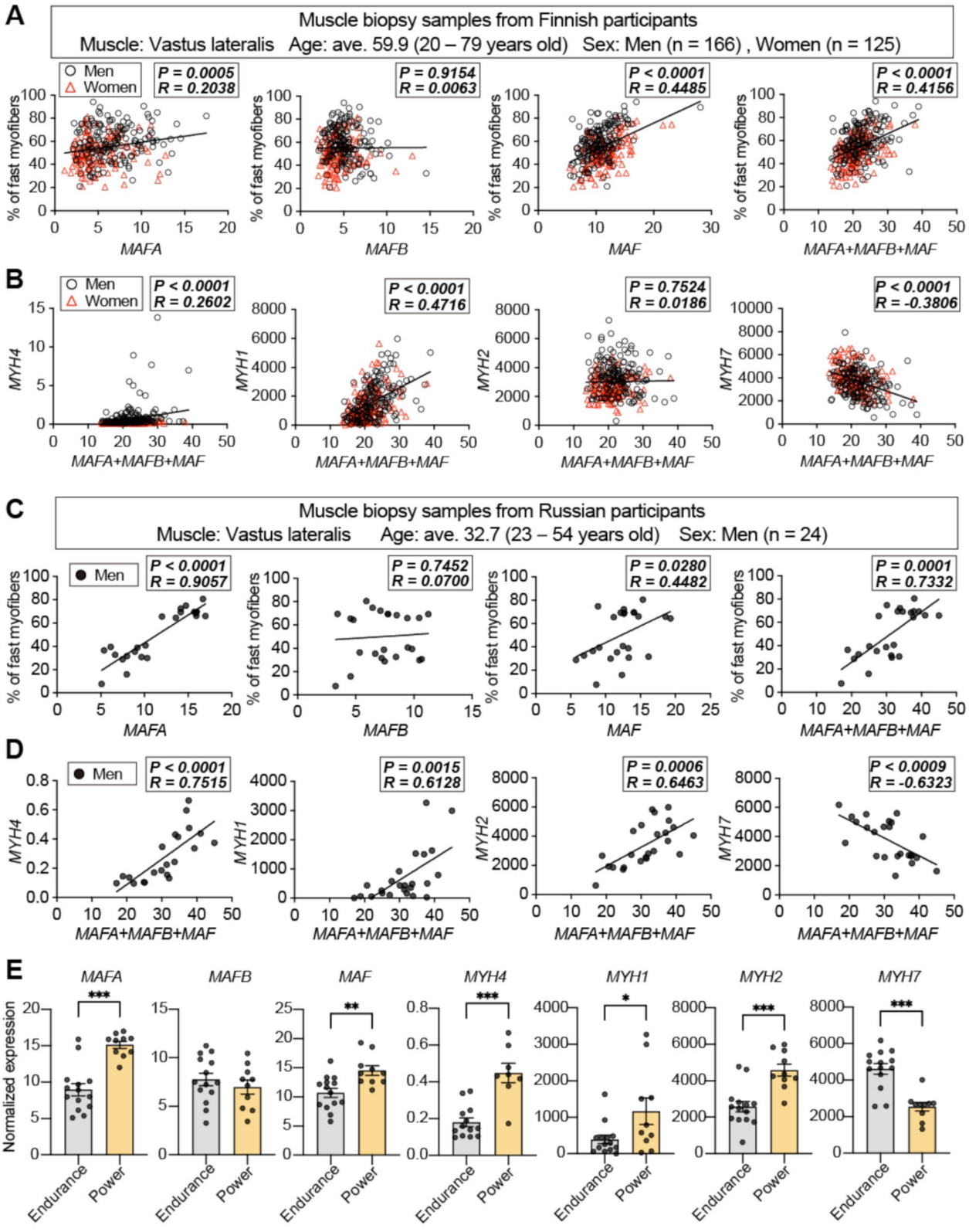

Fig. 5 (See legend on next page.)

(See figure on previous page.)

Fig. 5 Analysis of human skeletal muscle biopsy samples reveals a positive correlation between MYH4 and large MAF expression, highlighting the potential functionality of large MAFs in human skeletal muscle tissue. (**A-B**) Muscle biopsy samples were obtained from the vastus lateralis of 291 individuals in Finland, comprising 166 men and 125 women aged 20–79 years (mean age: 59.9 years). (**A**) Scatter plots showing the percentage of fast-twitch myofibers (y-axis) against the mRNA expression levels of *MAFA*, *MAFB*, *MAF*, or total large MAFs (*MAFA* + *MAFB* + *MAF*) (x-axis) for each participant, as determined using RNA-seq analysis. (**B**) Scatter plots showing the mRNA expression levels of *MYH4*, *MYH1*, *MYH2*, or *MYH7* (y-axis) against the total mRNA expression levels of large MAFs (*MAFA* + *MAFB* + *MAF*) (x-axis) for all 291 participants. (**C-D**) Muscle biopsy samples were obtained from the vastus lateralis of 24 men in Russia. The ages of the participants ranged from 20 to 45 years (mean age: 32.7 years). (**C**) Scatter plots showing the percentage of fast-twitch myofibers (y-axis) against the mRNA expression levels of *MAFA*, *MAFB*, *MAF*, or total large MAFs (*MAFA* + *MAFB* + *MAF*) (x-axis) for each participant, as determined through immunohistochemical and RNA-seq analyses. (**D**) Scatter plots showing the mRNA expression levels of *MYH4*, *MYH1*, *MYH2*, or *MYH7* (y-axis) against the total mRNA expression levels of large MAFs (*MAFA* + *MAFB* + *MAF*) (x-axis) for all 24 participants. (**E**) RNA-seq analysis of MAFA, MAFB, MAF, MYH4, MYH1, MYH2, and MYH7 expression in Russian muscle biopsy samples, categorized by training type: endurance training ($n = 14$) and power training ($n = 10$). *P* values were calculated using a two-sided Pearson correlation test (**A-D**) and Student's *t*-test (**E**); $^{*}P < 0.05$, $^{**}P < 0.01$, $^{***}P < 0.001$, R; Pearson correlation coefficient. Outliers were identified using Grubbs' test (Alpha = 0.05); three participants with outlying *MYH4* expression levels were excluded from the analysis (**D-E**)

regulate the fast-glycolytic gene program, consequently driving the acquisition of type IIb myofiber-like functional characteristics in human skeletal muscle.

Large MAF expression levels determine MYH4 expression in human skeletal muscle tissue

To confirm the association between large MAF and *MYH4* expression in human skeletal muscle tissue, we analyzed *MAFA*, *MAFB*, and *MAF* expression, as well as the combined expression of total large MAFs, using RNA-seq data and myofiber type proportions obtained from the muscle biopsies of 291 Finnish participants (men: $n = 166$, women: $n = 125$) (Fig. 5A, B) and 24 men Russian participants (Fig. 5C, D). In the Finnish cohort, we observed a clear positive correlation between the expression levels of *MAFA*, *MAF*, and total large MAFs and the percentage of fast type II myofibers regardless of sex (Fig. 5A). However, *MAFB* expression showed no significant correlation with the percentage of type II myofibers (Fig. 5A). Additionally, total large MAF expression levels were positively correlated with fast *MYH4* and *MYH1* (Fig. 5B); however, *MYH4* expression levels were markedly low. In contrast, total large MAF expression levels were negatively correlated with *MYH7* expression (Fig. 5B). Furthermore, analysis of each large MAF association with *MYH* genes revealed that *MAFA* and *MAF* showed a positive correlation with *MYH4* (Fig. S4A) and *MYH1* (Fig. S4B) and a negative correlation with *MYH7* (Fig. S4D). The expression levels of *MAFB* did not correlate with those of *MYH* genes, except for *MYH2* (Fig. S4C).

Similar correlation patterns were obtained in the muscle biopsy data from Russian samples compared to the Finnish dataset (Fig. 5C, D). Specifically, we detected a clear positive correlation between the expression levels of *MAFA*, *MAF*, and total large MAFs and the percentage of fast type II myofibers in the muscle samples of Russian participants, as quantified through immunostaining (Fig. 5C). Consistent with the samples obtained from Finnish participants, *MAFB* showed no correlation with the percentage of type II myofibers in the Russian dataset (Fig. 5C). Furthermore, total large MAF expression levels showed the strongest positive correlation with fast MYH (*MYH4*, *MYH1*, and *MYH2*) but was negatively correlated with the slow MYH, *MYH7*, in the Russian cohort (Fig. 5D). Analysis of individual large MAF associations with *MYH* genes revealed a similar trend: *MAFA* and *MAF* expression levels, but not *MAFB*, were positively correlated with *MYH4*, *MYH1*, and *MYH2* and negatively associated with *MYH7* (Fig. S5A-D). Although *MYH4* expression levels were considerably low across all samples compared to other *MYH* genes, our comprehensive analysis further confirm that large MAFs regulate *MYH4* expression in human skeletal muscle in vivo.

Lastly, we examined transcriptomic data from individuals with different training backgrounds to explore the relationship between large MAF expression and training-associated myofiber type profiles. A Russian dataset documenting physical activity was categorized into two groups: endurance-trained and power-trained participants. RNA-seq analysis revealed that *MAFA* and *MAF* expression levels were significantly higher in power-trained participants than in endurance-trained participants, whereas *MAFB* expression remained similar between the groups (Fig. 5E). Consistent with this result, the expression of fast *MYH* genes, including *MYH4*, was higher in power-trained individuals than in their endurance-trained counterparts, whereas slow-type *MYH7* was elevated in endurance-trained participants. Although the cross-sectional nature of the data limits causal interpretation, these results suggest that individuals with higher expression of MAFA and MAF—either due to genetic predisposition or training effects—tend to exhibit a fast-twitch dominant muscle phenotype.

Discussion

The limb skeletal muscles of small animals such as mice and rats predominantly comprise fast-twitch myofibers, including types IIa (*Myh2)*, IIx (*Myh1*), and IIb (*Myh4*). In contrast, human skeletal muscle lacks type IIb myofibers (*MYH4*), the fastest glycolytic myofiber type in the limb muscles of mammals [2, 4]. The present study builds

on our previous findings that large Mafs are a principal regulator of type IIb myofiber specification in mice [28]. In this study, large MAFs specifically and robustly regulated the expression of type IIb myofiber-specific genes, including *MYH4*, in human and bovine skeletal muscle cells. These results provide strong evidence that the regulatory machinery controlling *MYH4* expression, as described in mice, is also present and functional in human skeletal muscle cells but is likely suppressed by unidentified mechanisms. This study also shows that large MAFs drive a substantial upregulation not only *MYH4* mRNA expression but also MYH4 protein expression in human skeletal muscle cells. Furthermore, large MAF expression positively correlated with the proportion of fast myofibers and fast myosin isoform expression, including MYH4, despite its relatively low abundance compared to that of MYH1 and MYH2 in human skeletal muscle tissues.

Our previous work revealed that large Mafs (*Mafa*, *Mafb*, and *Maf*) specifically bind to the MARE sequence in the *Myh4* promoter, which is essential for the formation of type IIb myofibers in mice [28]. Because large mammals, including horses, cattle, and humans, have lost type IIb myofibers and *MYH4* expression for reasons that remain unclear, we hypothesized that reduced large MAF expression contributes to the evolutionary silencing of *MYH4* in these species.

In the present study, species with lower large *MAF* expression levels also exhibited reduced *MYH4* expression. However, this correlation was not completely consistent across all species. For example, *MYH4* expression remains extremely low despite non-negligible levels of large *MAF* transcripts in human skeletal muscle. This discrepancy suggests that additional regulatory mechanisms, such as post-transcriptional or epigenetic suppression, may contribute to *MYH4* silencing independently of large MAF transcript abundance. These findings indicate that, although large *MAF* mRNA levels may be a useful predictor of *MYH4* expression across species, their mRNA expression alone is likely insufficient to explain the transcriptional silencing of *MYH4* in human skeletal muscles.

Large MAF activity is regulated through multiple mechanisms, including transcriptional and translational controls, as well as regulation by microRNAs [59]. MYOD is a potential regulator of mouse *Mafb* and *Maf* promoter activity, as shown by luciferase assays [60, 61]. Additionally, MYOD binds to the *Mafa* promoter region in C2C12 cells, a mouse myoblast cell line (data not shown). However, *MYOD* expression was not downregulated in human myotubes in the present study (Fig. S3B). This suggests that the low expression of large MAFs in human skeletal muscle cannot be attributed to *MYOD* dynamics alone. A novel mechanism underlying the regulation of *Maf* expression was recently proposed in mice; *Maf* expression was significantly reduced in mice lacking *Cacna1s*, which encodes the α1s subunit of Cav1.1 [57]. As the rapidity of calcium transients varies among animal species [62], the diversity of calcium signaling or differences in *Cacna1s* expression across species may affect *Maf* expression levels.

Post-transcriptional regulation of large MAFs may partially explain the reduced expression of large MAF mRNA and protein in humans. miR-155 and miR-1290 interact with the 3′UTR of *Maf* in laryngeal squamous cell carcinoma [59, 63, 64]. miR-1290 is exclusively detected in great apes, including humans [59, 65]. This demonstrates the possibility of human-specific mechanisms that suppress *Maf* expression, such as those mediated by miR-1290. Additionally, epigenetic modifications, such as differences in histone acetylation or DNA methylation at the *Maf* locus, may contribute to the low expression of *Maf* observed in humans and other large mammals. However, further investigations are required to elucidate these potential mechanisms.

In addition to the low levels of large MAFs in human skeletal muscle, other suppressive mechanisms regulating *MYH4* may exist in humans. Nucleotide differences in the *MYH4* promoter between humans and mice may reduce transcriptional activity by disrupting the binding sites for MEF2 and serum response factor [66, 67]. Although this hypothesis provides an interesting perspective, our results challenge its relevance. Specifically, all *MAFA*, *MAFB*, and *MAF* markedly upregulated *MYH4* expression in human myotubes, despite the reported differences in the *MYH4* promoter region. Furthermore, the MARE, a key binding site for large MAFs, was highly conserved across animal species (Fig. 1B). This result confirms that the MARE region in the human *MYH4* promoter retains its functional relevance regardless of the nucleotide differences highlighted in the previous study. Thus, large MAFs can likely override the effects of these promoter differences, directly activating *MYH4* expression in human myotubes. Therefore, we propose that the nucleotide differences in the *MYH4* promoter are unlikely to fully account for the low expression of *MYH4* in humans.

An fMyh-SE region located 42 kb upstream of the *Myh2-Myh1-Myh4* fast myosin gene cluster was recently identified as a critical regulator of fast myosin gene expression in mice [27, 68]. Dos Santos et al. [27] and Sakakibara et al. [68] demonstrated that the fMyh-SE region interacts exclusively with each *fMyh* promoter through a 3D chromatin looping structure, thereby enabling precise and robust expression of specific fast myosin genes. Although our previous and present studies have identified large MAFs as specific transcriptional regulators of *Myh4* (*MYH4*) in both mice and humans, the transcription factors specifically regulating *Myh1* and

Myh2 remain unknown. Given the exclusive regulation mediated by fMyh-SE, we hypothesize that transcription factors specific to *MYH1* or *MYH2* preferentially dominate the fMyh-SE region in humans. This dominance could restrict access to *MYH4*, thereby contributing to its low expression in human skeletal muscle. However, our findings suggest that overexpression of large MAFs can override this exclusivity. Large MAFs may "hijack" the fMyh-SE region to induce *MYH4* expression even in human skeletal muscle, where endogenous large MAF expression is low. This model highlights the complex interplay between super-enhancer regulation and transcription factor specificity during the regulation of myosin gene expression across species, which partially explains why the human skeletal muscle has lost *MYH4* expression.

MYH4 mRNA was previously detected in a small subset of specialized muscles, such as the human masseter and laryngeal muscles, as well as in skeletal muscle from patients with Duchenne muscular dystrophy [25, 50, 66]. Although single-fiber proteomics have revealed low levels of MYH4 peptides in fast human muscle fibers [17], there remains no definitive evidence of MYH4 expression under defined regulatory conditions. The present study provides the first functional demonstration of the activation of MYH4 expression through overexpression of each large *MAF* in human skeletal muscle cells.

Type IIb myofibers, which are characterized by their fast contraction speeds and high force generation, also have the highest concentration of glycolytic enzymes compared to other type II myofibers. One of the limitations of the present study is that it did not determine whether the induction of type IIb myofibers is beneficial or detrimental to human skeletal muscle or overall health. However, our reanalysis of snRNA-seq in human skeletal muscle [16] demonstrated that fast myofiber signatures, including fast MYH, are preferentially lost with aging, along with a decline in *MAF* expression. Furthermore, shifts in myofiber types, whether in pathological or physiological contexts, can affect the skeletal muscle microenvironment, including vasculature, the extracellular matrix, the stem cell niche, and MuSCs. Thus, we hypothesize that restoring MAF expression could counteract the pathological features of sarcopenia by improving muscle mass and function, and by rejuvenating the microenvironment of aged skeletal muscle. This could include enhancing MuSC-mediated regeneration, ultimately providing a comprehensive approach for mitigating the detrimental effects of aging on skeletal muscle.

Large MAFs specifically activated type IIb-specific genes and glycolytic-associated gene programs, suggesting that they exhibit some functional redundancy in the activation of these gene sets. They commonly downregulated the expression of members of the MEF2 family (*MEF2A*, *MEF2B*, and *MEF2C*) that contribute to the transcription of slow oxidative myofiber-specific gene programs [69–72]. Furthermore, the overexpression of *Smarcd3*, which encodes BAF60c, in mouse skeletal muscle strongly promotes glycolytic gene expression and enhances insulin sensitivity [55]. In contrast, large MAFs downregulated *SMARCD3* expression in human myotubes in our study. This suggests that large MAFs regulate glycolytic genes independently of *SMARCD3*. Consistent with this, we identified MARE sequences in the promoters of all glycolysis-related genes listed in Fig. 4H, indicating the direct regulatory role of large MAFs in glycolytic gene activation.

Our RNA-seq analysis of myotubes overexpressing each large MAF also revealed distinct functional signatures for each transcription factor. For instance, pathways related to the ubiquitin-dependent protein catabolic process and protein transport were specifically enriched in MAFA-overexpressing myotubes, whereas pathways associated with interferon beta production and innate immune response were enriched in MAFB-overexpressing myotubes (Fig. S2A, B). Cytoplasmic translation and ribosomal biogenesis pathways were prominently enriched in MAF-overexpressing myotubes (Fig. S2C). Although MAFA induced *MYH4* expression to a lesser extent than MAFB or MAF (Figs. 2G-H and 4C), it equally promoted the expression of most glycolytic genes (Fig. 4H). These findings indicate that large MAFs have unique targets and preferences despite their shared role in the activation of type IIb-specific and glycolytic gene programs. Therefore, future studies should explore co-transcriptional factors and chromatin remodeling complexes that interact with each large MAF to further explore how large MAFs orchestrate diverse gene programs in mice and human skeletal muscle.

Our in vitro findings were further validated in vivo using RNA-seq data from human muscle biopsy samples. Despite the low expression levels of *MYH4*, a clear positive correlation was observed between *MYH4* expression and the expression of *MAFA*, *MAF*, or total large MAFs across two independent cohorts. The expression of *MYH1*, which encodes type IIx myosin, was also positively correlated with *MAFA*, *MAF*, and total large MAFs in both cohorts. Unlike mouse and rat skeletal muscle, human type IIx myofibers exhibit the fastest contraction speeds and the highest glycolytic activity, while showing the lowest succinate dehydrogenase activity [2, 17, 73]. In the present study, large MAFs did not directly induce *MYH1* expression but strongly upregulated the expression of glycolytic genes. Therefore, we hypothesize that the observed correlation between *MYH1* and large MAF expression reflects the role of large MAFs in driving glycolytic gene programs, specifically in fast-glycolytic fibers such as type IIx myofibers. The associations between

large MAFs and fast myofiber characteristics are further supported by a recent single-cell regulatory network analysis by Moreno-Justicia et al. [23], which identified *MAFA* and *MAF* as the specific transcription factors for fast-type myofibers based on SCENIC-derived regulon specificity scores. This independent, regulon-based analysis reinforces the relevance of large *MAFs*—particularly *MAFA* and *MAF*—in defining the fast-glycolytic transcriptional program in human skeletal muscle.

RNA-seq analysis of the data of Russian participants also revealed that large MAF expression differs depending on the training regimen. *ACTN3*, a key gene associated with athletic speed, showed the strongest positive correlation with *MAF* expression in humans. As the *ACTN3* promoter contains a MARE site, *MAFA* and *MAF* expression levels may serve as potential biomarkers for guiding individuals toward sports that align with their muscle fiber characteristics. Furthermore, our findings suggest that certain individuals, such as professional athletes, may naturally exhibit higher levels of large MAFs or possess gain-of-function genetic variants that promote the development of type IIb-like muscle traits. Therefore, future studies should investigate these genetic variants across diverse populations to elucidate their role in a muscle performance and muscle fiber specialization.

In conclusion, our findings establish large MAFs as key regulators of fast glycolytic myofiber programs across mammals and suggest that they may unlock a latent potential for type IIb myofiber development in humans. However, whether this molecular activation translates into enhanced muscle contractility or power remains unknown. Given that fast-twitch fibers are preferentially lost during aging, further studies are required to determine whether modulating large MAF activity can help preserve fast muscle traits in humans while accounting for the complexity of the human motor system.

Supplementary Information

The online version contains supplementary material available at https://doi.org/10.1186/s13395-025-00391-5.

Supplementary Material 1

Acknowledgements

We would like to thank Dr. Pascal Maire (Institut Cochin, INSERM, France) and Dr. Stefano Schiaffino (University of Padova, Italy) for their insightful comments on our study. We also thank Ms. Aki Matsumoto (Kyoto University) for technical assistance with cell culture and sorting and Dr. Takashi Matsuzaka (University of Tsukuba) for technical support with the Seahorse flux analyzer. We thank the FRCC PCM "Genomics, Proteomics, and Metabolomics" Center for their assistance with RNA sequencing. We also thank Dr. Tsuchimoto and Dr. Kodama (Aichi Medical University, Institute of Comprehensive Medical Research, Division of Advanced Research Promotion) for their assistance with Zeno SWATH-MS data acquisition.

Author contributions

Methodology: SS, RF Investigation: SS, RT, TH, RI, MW, GW, IS, KO, TK, HS, MM, EAS, RIS, AVZ, EVG, IIA, RF Writing—original draft: SS, RF Funding acquisition: SS, KO, IIA, HS, ST, RF Conceptualization: SS, RF All authors read and approved the final manuscript.

Funding

AMED-CREST grant JP23gm171008h (RF, ST). Japan Society for the Promotion of Science (JSPS) grants 24K02876 (RF), 24K22244 (RF), and 21K19195 (KO). Takeda Science Foundation (RF). Mochida Memorial Foundation for Medical and Pharmaceutical Research grant (RF). JST FOREST program JPMJFR234V (RF). Russian Science Foundation grant 24-15-00413 (IIA). Acceleration Program for Intractable Diseases Research utilizing Disease-specific iPS cells grant JP20bm0804025 (HS). JSPS Research Fellowships for Young Scientists grant 23KJ0287 (SS).

Data availability

Data and materials availability: All unique reagents generated in this study are available from the corresponding author, Ryo Fujita (fujiryo@md.tsukuba.ac.jp), in accordance with the relevant material transfer agreements. RNA-seq data of human iMuSC-derived myotubes are available in the NCBI Gene Expression Omnibus (GEO) database under accession number "GSE283853". RNA-seq data of human biopsy are available in the NCBI Gene Expression Omnibus (GEO) database and the Database of Genotypes and Phenotypes under accession numbers "GSE200398" and "phs001048.v2.p1", respectively. LC-MS/MS data have been deposited to the Proteome Xchange Consortium via jPOSTrepo with the dataset identifier JPST003487. This paper does not report original code. Any additional information required to reanalyze the data reported in this paper is available from the corresponding author, Ryo Fujita (fujiryo@md.tsukuba.ac.jp) upon request.

Declarations

Ethics approval and consent to participate

The Russian part of the study was approved by the Ethics Committee of the Federal Research and Clinical Center of Physical–Chemical Medicine of the Federal Medical and Biological Agency of Russia (protocol no. 2017/04), whereas the Finnish part of the study was approved by the Hospital District of Helsinki and Uusimaa (Database of Genotypes and Phenotypes Study Accession: phs001048.v2.p1). Written informed consent was obtained from all study participants.

Consent for publication

Not applicable.

Competing interests

TK and ST are inventors on a patent application related to this work (Patent Application No. 2022-083553). All other authors declare they have no competing interests.

Author details

[1]Laboratory Animal Resource Center in Transborder Medical Research Center, Department of Anatomy and Embryology, Institute of Medicine, University of Tsukuba, Ibaraki 305-8575, Japan
[2]Université Paris Est Créteil, Institut National de la Santé et de la Recherche Médicale (INSERM), Mondor Institute for Biomedical Research (IMRB), Créteil, France
[3]Department of Artificial Intelligence Medicine, Graduate School of Medicine, Chiba University, Chiba, Japan
[4]Department of Molecular Biology and Genetics, Lopukhin Federal Research and Clinical Center of Physical-Chemical Medicine of Federal Medical Biological Agency, Moscow 119435, Russia
[5]Research Institute of Physical Culture and Sport, Sport and Tourism, Volga Region State University of Physical Culture, Kazan 420138, Russia
[6]Laboratory of Genetics of Aging and Longevity, Kazan State Medical University, Kazan 420012, Russia
[7]Research Institute for Sport and Exercise Sciences, Liverpool John Moores University, Liverpool L3 5AF, UK
[8]Department of Physiology, School of Medicine, Aichi Medical University, Nagakute, Aichi, Japan
[9]Division of Animal Products Research, NARO Institute of Livestock and Grassland Science, Tsukuba 305-0901, Ibaraki, Japan
[10]Department of Clinical Application, Center for iPS Cell Research and Application (CiRA), Kyoto University, Kyoto 606-8507, Japan

[11]Department of Genome Biology, Transborder Medical Research Center, Institute of Medicine, University of Tsukuba, Ibaraki 305- 8575, Japan
[12]Division of Regenerative Medicine, Transborder Medical Research Center, Institute of Medicine, University of Tsukuba, Ibaraki 305-8575, Japan

Received: 28 March 2025 / Accepted: 16 July 2025
Published online: 26 July 2025

References

1. Ciciliot S, Rossi AC, Dyar KA, Blaauw B, Schiaffino S. Muscle type and fiber type specificity in muscle wasting. Int J Biochem Cell Biol. 2013;45:2191–9.
2. Schiaffino S, Reggiani C. Fiber types in mammalian skeletal muscles. Physiol Rev. 2011;91:1447–531.
3. Bottinelli R, Canepari M, Pellegrino MA, Reggiani C. Force-velocity properties of human skeletal muscle fibres: myosin heavy chain isoform and temperature dependence. J Physiol. 1996;495:573–86.
4. Schiaffino S, Chemello F, Reggiani C. The diversity of skeletal muscle Fiber types. Cold Spring Harb Perspect Biol. 2024;a041477.
5. Albers PH, Pedersen AJT, Birk JB, Kristensen DE, Vind BF, Baba O, et al. Human muscle fiber type-specific insulin signaling: impact of obesity and type 2 diabetes. Diabetes. 2015;64:485–97.
6. Schuler M, Ali F, Chambon C, Duteil D, Bornert J-M, Tardivel A, et al. PGC1α expression is controlled in skeletal muscles by PPARβ, whose ablation results in fiber-type switching, obesity, and type 2 diabetes. Cell Metab. 2006;4:407–14.
7. Selsby JT, Morine KJ, Pendrak K, Barton ER, Sweeney HL. Rescue of Dystrophic Skeletal Muscle by PGC-1α Involves a Fast to Slow Fiber Type Shift in the mdx Mouse. Carvalho DP de, editor. PLoS ONE. 2012;7:e30063.
8. Reyes NL, Banks GB, Tsang M, Margineantu D, Gu H, Djukovic D, et al. Fnip1 regulates skeletal muscle fiber type specification, fatigue resistance, and susceptibility to muscular dystrophy. Proc Natl Acad Sci. 2015;112:424–9.
9. Hayashi T, Fujita R, Okada R, Hamada M, Suzuki R, Fuseya S, et al. Lunar gravity prevents skeletal muscle atrophy but not myofiber type shift in mice. Commun Biol. 2023;6:424.
10. Jerkovic R, Argentini C, Serrano-Sanchez A, Cordonnier C, Schiaffino S. Early myosin switching induced by nerve activity in regenerating slow skeletal muscle. Cell Struct Funct. 1997;22:147–53.
11. Shimizu J, Kawano F. Exercise-induced histone H3 trimethylation at lysine 27 facilitates the adaptation of skeletal muscle to exercise in mice. J Physiol. 2022;600:3331–53.
12. Furrer R, Heim B, Schmid S, Dilbaz S, Adak V, Nordström KJV, et al. Molecular control of endurance training adaptation in male mouse skeletal muscle. Nat Metab. 2023;5:2020–35.
13. Lin J, Wu H, Tarr PT, Zhang C-Y, Wu Z, Boss O, et al. Transcriptional co-activator PGC-1α drives the formation of slow-twitch muscle fibres. Nature. 2002;418:797–801.
14. Larsson L, Biral D, Campione M, Schiaffino S. An age-related type IIB to IIX myosin heavy chain switching in rat skeletal muscle. Acta Physiol Scand. 1993;147:227–34.
15. Petrany MJ, Swoboda CO, Sun C, Chetal K, Chen X, Weirauch MT, et al. Single-nucleus RNA-seq identifies transcriptional heterogeneity in multinucleated skeletal myofibers. Nat Commun. 2020;11:6374.
16. Lai Y, Ramírez-Pardo I, Isern J, An J, Perdiguero E, Serrano AL, et al. Multimodal cell atlas of the ageing human skeletal muscle. Nature. 2024;629:154–64.
17. Murgia M, Toniolo L, Nagaraj N, Ciciliot S, Vindigni V, Schiaffino S, et al. Single muscle Fiber proteomics reveals Fiber-Type-Specific features of human muscle aging. Cell Rep. 2017;19:2396–409.
18. Wang L, Gao P, Li C, Liu Q, Yao Z, Li Y, et al. A single-cell atlas of bovine skeletal muscle reveals mechanisms regulating intramuscular adipogenesis and fibrogenesis. J Cachexia Sarcopenia Muscle. 2023;14:2152–67.
19. Wang L, Zhou Y, Wang Y, Shan T. Integrative cross-species analysis reveals conserved and unique signatures in fatty skeletal muscles. Sci Data. 2024;11:290.
20. Pellegrino MA, Canepari M, Rossi R, D'Antona G, Reggiani C, Bottinelli R. Orthologous myosin isoforms and scaling of shortening velocity with body size in mouse, rat, rabbit and human muscles. J Physiol. 2003;546:677–89.
21. Smerdu V, Karsch-Mizrachi I, Campione M, Leinwand L, Schiaffino S. Type IIx myosin heavy chain transcripts are expressed in type IIb fibers of human skeletal muscle. Am J Physiol-Cell Physiol. 1994;267:C1723–8.
22. Murach KA, Dungan CM, Kosmac K, Voigt TB, Tourville TW, Miller MS, et al. Fiber typing human skeletal muscle with fluorescent immunohistochemistry. J Appl Physiol. 2019;127:1632–9.
23. Van Der Moreno-Justicia R, Stocks B, Laitila J, Van De Seaborne RA, et al. Human skeletal muscle fiber heterogeneity beyond myosin heavy chains. Nat Commun. 2025;16:1764.
24. Stirn Kranjc B, Smerdu V, Eržen I. Histochemical and immunohistochemical profile of human and rat ocular medial rectus muscles. Graefes Arch Clin Exp Ophthalmol. 2009;247:1505–15.
25. Horton MJ, Rosen C, Close JM, Sciote JJ. Quantification of myosin heavy chain RNA in human laryngeal muscles: differential expression in the vertical and horizontal posterior cricoarytenoid and thyroarytenoid. Laryngoscope. 2008;118:472–7.
26. Bloemberg D, Quadrilatero J. Rapid determination of myosin heavy chain expression in rat, mouse, and human skeletal muscle using multicolor Immunofluorescence analysis. PLoS ONE. 2012;7:e35273.
27. Dos Santos M, Backer S, Auradé F, Wong MM-K, Wurmser M, Pierre R, et al. A fast myosin super enhancer dictates muscle fiber phenotype through competitive interactions with myosin genes. Nat Commun. 2022;13:1039.
28. Sadaki S, Fujita R, Hayashi T, Nakamura A, Okamura Y, Fuseya S, et al. Large Maf transcription factor family is a major regulator of fast type IIb myofiber determination. Cell Rep. 2023;42:112289.
29. Okita K, Matsumura Y, Sato Y, Okada A, Morizane A, Okamoto S, et al. A more efficient method to generate integration-free human iPS cells. Nat Methods. 2011;8:409–12.
30. Zhao M, Taniguchi Y, Shimono C, Jonouchi T, Cheng Y, Shimizu Y, et al. Heparan sulfate Chain-Conjugated Laminin-E8 fragments advance paraxial mesodermal differentiation followed by high myogenic induction from HiPSCs. Adv Sci. 2024;11:2308306.
31. Kawada R, Jonouchi T, Kagita A, Sato M, Hotta A, Sakurai H. Establishment of quantitative and consistent in vitro skeletal muscle pathological models of myotonic dystrophy type 1 using patient-derived iPSCs. Sci Rep. 2023;13:94.
32. Nalbandian M, Zhao M, Sasaki-Honda M, Jonouchi T, Lucena-Cacace A, Mizusawa T, et al. Characterization of hiPSC-Derived muscle progenitors reveals distinctive markers for myogenic cell purification toward cell therapy. Stem Cell Rep. 2021;16:883–98.
33. Fujita R, Mizuno S, Sadahiro T, Hayashi T, Sugasawa T, Sugiyama F, et al. Generation of a myod knock-in reporter mouse line to study muscle stem cell dynamics and heterogeneity. iScience. 2023;26:106592.
34. Hayashi T, Sadaki S, Tsuji R, Okada R, Fuseya S, Kanai M et al. Dual-specificity phosphatases 13 and 27 as key switches in muscle stem cell transition from proliferation to differentiation. Stem Cells Dayt Ohio. 2024;sxae045.
35. Muroya S, Nakajima I, Chikuni K. Sequential expression of myogenic regulatory factors in bovine skeletal muscle and the satellite cell culture. Anim Sci J. 2002;73:375–81.
36. Ojima K, Uezumi A, Miyoshi H, Masuda S, Morita Y, Fukase A, et al. Mac-1low early myeloid cells in the bone marrow-derived SP fraction migrate into injured skeletal muscle and participate in muscle regeneration. Biochem Biophys Res Commun. 2004;321:1050–61.
37. Minati L, Firrito C, Del Piano A, Peretti A, Sidoli S, Peroni D et al. One-shot analysis of translated mammalian lncRNAs with AHARIBO. Chang HY, Manley JL, Rinn JL, editors. eLife. 2021;10:e59303.
38. Huang DW, Sherman BT, Lempicki RA. Systematic and integrative analysis of large gene lists using DAVID bioinformatics resources. Nat Protoc. 2009;4:44–57.
39. Alquicira-Hernandez J, Powell JE. Nebulosa recovers single-cell gene expression signals by kernel density estimation. Mathelier A, editor. Bioinformatics. 2021;37:2485–7.
40. Demichev V, Messner CB, Vernardis SI, Lilley KS, Ralser M. DIA-NN: neural networks and interference correction enable deep proteome coverage in high throughput. Nat Methods. 2020;17:41–4.
41. Okuda S, Watanabe Y, Moriya Y, Kawano S, Yamamoto T, Matsumoto M, et al. jPOSTrepo: an international standard data repository for proteomes. Nucleic Acids Res. 2017;45:D1107–11.
42. Bastian FB, Roux J, Niknejad A, Comte A, Fonseca Costa SS, de Farias TM, et al. The Bgee suite: integrated curated expression atlas and comparative transcriptomics in animals. Nucleic Acids Res. 2021;49:D831–47.
43. Grant CE, Bailey TL, Noble WS. FIMO: scanning for occurrences of a given motif. Bioinformatics. 2011;27:1017–8.
44. Taylor DL, Jackson AU, Narisu N, Hemani G, Erdos MR, Chines PS, et al. Integrative analysis of gene expression, DNA methylation, physiological

traits, and genetic variation in human skeletal muscle. Proc Natl Acad Sci. 2019;116:10883–8.
45. Bray NL, Pimentel H, Melsted P, Pachter L. Near-optimal probabilistic RNA-seq quantification. Nat Biotechnol. 2016;34:525–7.
46. Soneson C, Love MI, Robinson MD. Differential analyses for RNA-seq: transcript-level estimates improve gene-level inferences. F1000Research. 2016;4:1521.
47. Harrow J, Frankish A, Gonzalez JM, Tapanari E, Diekhans M, Kokocinski F, et al. GENCODE: the reference human genome annotation for the ENCODE project. Genome Res. 2012;22:1760–74.
48. Anders S, Pyl PT, Huber W. HTSeq—a Python framework to work with high-throughput sequencing data. Bioinformatics. 2015;31:166–9.
49. Zhao M, Tazumi A, Takayama S, Takenaka-Ninagawa N, Nalbandian M, Nagai M, et al. Induced fetal human muscle stem cells with high therapeutic potential in a mouse muscular dystrophy model. Stem Cell Rep. 2020;15:80–94.
50. Horton MJ, Brandon CA, Morris TJ, Braun TW, Yaw KM, Sciote JJ. Abundant expression of myosin heavy-chain IIB RNA in a subset of human masseter muscle fibres. Arch Oral Biol. 2001;46:1039–50.
51. Grifone R, Laclef C, Spitz F, Lopez S, Demignon J, Guidotti J-E, et al. Six1 and Eya1 expression can reprogram adult muscle from the Slow-Twitch phenotype into the Fast-Twitch phenotype. Mol Cell Biol. 2004;24:6253–67.
52. Niro C, Demignon J, Vincent S, Liu Y, Giordani J, Sgarioto N, et al. Six1 and Six4 gene expression is necessary to activate the fast-type muscle gene program in the mouse primary myotome. Dev Biol. 2010;338:168–82.
53. Hetzler KL, Collins BC, Shanely RA, Sue H, Kostek MC. The homoeobox gene SIX1 alters myosin heavy chain isoform expression in mouse skeletal muscle. Acta Physiol. 2014;210:415–28.
54. Lee KY, Singh MK, Ussar S, Wetzel P, Hirshman MF, Goodyear LJ, et al. Tbx15 controls skeletal muscle fibre-type determination and muscle metabolism. Nat Commun. 2015;6:8054.
55. Meng Z-X, Li S, Wang L, Ko HJ, Lee Y, Jung DY, et al. Baf60c drives glycolytic metabolism in the muscle and improves systemic glucose homeostasis through Deptor-mediated Akt activation. Nat Med. 2013;19:640–5.
56. Nabeshima Y, Hanaoka K, Hayasaka M, Esuml E, Li S, Nonaka I, et al. Myogenin gene disruption results in perinatal lethality because of severe muscle defect. Nature. 1993;364:532–5.
57. Dos Santos M, Shah AM, Zhang Y, Bezprozvannaya S, Chen K, Xu L, et al. Opposing gene regulatory programs governing myofiber development and maturation revealed at single nucleus resolution. Nat Commun. 2023;14:4333.
58. Correia JC, Kelahmetoglu Y, Jannig PR, Schweingruber C, Shvaikovskaya D, Zhengye L, et al. Muscle-secreted neurturin couples myofiber oxidative metabolism and slow motor neuron identity. Cell Metab. 2021;33:2215–e22308.
59. Deng Y, Lu L, Zhang H, Fu Y, Liu T, Chen Y. The role and regulation of Maf proteins in cancer. Biomark Res. 2023;11:17.
60. Huang K, Serria MS, Nakabayashi H, Nishi S, Sakai M. Molecular cloning and functional characterization of the mouse MafB gene. Gene. 2000;242:419–26.
61. Serria MS, Ikeda H, Omoteyama K, Hirokawa J, Nishi S, Sakai M. Regulation and differential expression of the c-maf gene in differentiating cultured cells. Biochem Biophys Res Commun. 2003;310:318–26.
62. Lee J-H, Lewis KM, Moural TW, Kirilenko B, Borgonovo B, Prange G, et al. Molecular parallelism in fast-twitch muscle proteins in echolocating mammals. Sci Adv. 2018;4:eaat9660.
63. Janiszewska J, Bodnar M, Paczkowska J, Ustaszewski A, Smialek MJ, Szylberg L, et al. Loss of the MAF transcription factor in laryngeal squamous cell carcinoma. Biomolecules. 2021;11:1035.
64. Na Y, Hall A, Choi K, Hu L, Rose J, Coover RA, et al. MicroRNA-155 contributes to plexiform neurofibroma growth downstream of MEK. Oncogene. 2021;40:951–63.
65. Yelamanchili SV, Morsey B, Harrison EB, Rennard DA, Emanuel K, Thapa I, et al. The evolutionary young miR-1290 favors mitotic exit and differentiation of human neural progenitors through altering the cell cycle proteins. Cell Death Dis. 2014;5:e982–982.
66. Harrison BC, Allen DL, Leinwand LA. IIb or not iib?? Regulation of myosin heavy chain gene expression in mice and men. Skelet Muscle. 2011;1:5.
67. Brown DM, Brameld JM, Parr T. Expression of the myosin heavy chain IIB gene in Porcine skeletal muscle: the role of the CArG-Box promoter response element. PLoS ONE. 2014;9:e114365.
68. Sakakibara I, Santolini M, Ferry A, Hakim V, Maire P. Six Homeoproteins and a linc-RNA at the Fast MYH Locus Lock Fast Myofiber Terminal Phenotype. Dawn C, editor. PLoS Genet. 2014;10:e1004386.
69. Chin ER, Olson EN, Richardson JA, Yang Q, Humphries C, Shelton JM, et al. A calcineurin-dependent transcriptional pathway controls skeletal muscle fiber type. Genes Dev. 1998;12:2499–509.
70. Liu L, Ding C, Fu T, Feng Z, Lee J-E, Xiao L, et al. Histone methyltransferase MLL4 controls myofiber identity and muscle performance through MEF2 interaction. J Clin Invest. 2020;130:4710–25.
71. Potthoff MJ, Wu H, Arnold MA, Shelton JM, Backs J, McAnally J, et al. Histone deacetylase degradation andMEF2 activation promote the formation of slow-twitch myofibers. J Clin Invest. 2007;117:2459–67.
72. Wu H. MEF2 responds to multiple calcium-regulated signals in the control of skeletal muscle fiber type. EMBO J. 2000;19:1963–73.
73. Schiaffino S. Fibre types in skeletal muscle: a personal account. Acta Physiol. 2010;199:451–63.

Publisher's note

mitigating fast-twitch fiber loss associated with aging and muscle degeneration.

Keywords MYH4, Type IIb myofiber, Myofiber type, Large MAFs, Myosin heavy chain, Aging, Human muscle